Present and future coastal flooding hazard for Long Island, NY and Long Island Sound (NY/CT), USA.

Authors: Salme Cook^{†*}and Liv Herdman[†]

† USGS, New York Water Science Center,
Troy, NY 12180, U.S.A.

Disclaimer: "This information product has been peer reviewed and approved for publication as a preprint by the U.S. Geological Survey."

^{*} Corresponding Author: secook@usgs.gov

Highlights:

- Regional analysis of coastal inundation and wave hazards
- An extreme value analysis of historical observations and climate model projections of non-tidal residuals (NTR) to predict changes in coastal flood hazard for Long Island, NY and Long Island Sound.
- A qualitative estimate of wave runup and wave overtopping discharge was used to evaluate the wave hazards for Long Island, NY and Long Island Sound.

Keywords:

- Extreme value analysis, regional coastal inundation, flood hazard, wave hazard

0.0 Abstract

Coastal flooding and the associated damages due to storms are increasing with sea level rise around the world, with regional variability in the severity of impacts., Researchers and resource managers need to better understand and predict the future shifts in coastal flooding due to these processes to plan for resilient and sustainable communities. Here we present an analysis of long-term historical records of water levels, tides, and modeled present-day wave climatologies, to characterize the present-day inundation extent in Long Island Sound and Long Island, NY. To understand the potential future changes in inundation extent, we provide a similar analysis of future climate projections of non-tidal residuals (storm surge) for the year 2050 and compare these projections with our present-day results. We examine both the magnitude of relatively frequent events with a 0.99 annual exceedance probability to more extreme events with a 0.01 annual exceedance probability (or the 1 in 100-year event). This range of events is relevant for local managers to understand the spatial variability in coastal inundation, in addition to planning for larger more catastrophic events.

1.0 Introduction

Coastal flooding due to storms and sea level rise is changing globally, although the associated hazards are not evenly distributed across the globe; regional variability in changing water levels from storms and sea level rise can contribute significantly to changes in hazardous flooding. Sea level rise is primarily driven by the addition of water mass to the oceans from ice sheets and glaciers and thermal expansion due to a warming climate (Sweet 2022). Regionally, sea level rise can vary from the average global rate from the uneven distribution of both the additional water mass and thermal expansion as well as coastal geology, post-glacial rebound, subsidence, and spatial variation in hydrodynamics (Mikolajewicz et al., 1990, Frederikse et al., 2020). In the United States, long-term historical data (over 180 gages with over 10-year records in addition to 30 years of satellite altimetry data; Sweet et al., 2022) are available to ascertain regional patterns in sea level rise. These broad patterns in sea level rise can be applied regionally; however, coastal

flooding also depends on storm dynamics, such as storm surge interaction with bathymetry and shoreline exposure to waves (Almar et al., 2021, Vitousek et al., 2017a). Many local-scale factors can affect coastal flooding from storms including the size and shape of the water body; the type, elevation, and slope of the shoreline; and the prevailing wind directions and atmospheric conditions associated with the storm itself.

One approach to quantifying coastal flood hazards can be to explicitly model coastal storms with mechanistic models (e.g., Couple Ocean Atmosphere Wave Sediment Transport Modeling system (COAWST), Warner et al., 2010, Coastal Storm Modeling System (CoSMoS), Barnard et al., 2014, Finite Volume Community Ocean Model (FVCOM), Chen et al., 2007); however, this a computationally expensive effort that can involve modeling a myriad of storms using an ensemble approach because the highest water levels across the region may be associated with different storm trajectories and dependent on shoreline orientation. An example of this approach is the North Atlantic Coast Comprehensive Study (NACCS; Cialone et al., 2015), which used observations to create synthetic tropical storm forcing for a regional model in the eastern United States. However, in NACCS, the storm surge model is too coarse to accurately simulate water levels in regions with highly variable shorelines (Liu et al., 2020). Another approach is to apply a statistical model to the time-series data to predict a frequency level associated with a particular condition, in this case extreme water levels. In hydrological flood frequency analysis, it is often standard to fit Generalized Extreme Value or Log Pearson type 3 distributions to annual maximum time series (Hu et al., 2020). As these techniques became more utilized in oceanography, a peaksover-threshold (POT) sampling method was identified as the more appropriate approach (Pickands, 1975, Mazas & Hamm, 2011, Nadal-Caraballo et al., 2016), and the Generalized Pareto Distribution (GPD) is commonly fit to the selected data (Davison & Smith, 1990).

Liu et al., 2020, combined these approaches and applied them to the Connecticut (CT) shoreline of Long Island Sound, New York (NY) using modeled water levels and significant wave heights from the 44 highest-ranked historical storms. They found that water levels for a given annual exceedance probability (AEP) were generally higher along the western coast of CT most likely due to the funnel shape of Long Island Sound. They found the inverse for significant wave height; for a given AEP, significant wave height increased eastward along the CT shoreline. This study Liu et al., 2020 highlighted the utility of the statistical approach in understanding coastal inundation and demonstrated the importance of understanding the combined impact and spatial variability of elevated water levels due to storm surge and storm induced waves when assessing the coastal flood hazards in a region.

To demonstrate how coastal hazards may evolve in a changing climate, numerical models, are often used. General Circulation Models (GCMs) are complex numerical models that simulate potential future climate change scenarios across the globe. Models that include tides, storm surge and annual change in mean sea level can be used to understand future coastal flood hazards because these factors can contribute to inundation along the coast (Nederhoff et al.,

2021). In these models, meteorological and atmospheric conditions are often based on a global climate projection, like the Coupled Model Intercomparison Project Phase 6 (CMIP6) global climate projection dataset from the High-Resolution Model Intercomparison Project (HighResMIP) multi-model ensemble (Haarsma et al., 2016). These high-resolution climate models are used to force higher resolution ocean and regional models like the Global Tide and Surge Model (GTSM) that includes dynamic interactions between tides, storm surges and changes in mean sea level. Published model water level datasets can be used in analyzing future non-tidal residual (storm surge) induced flooding at a finer scale; however, these models do not include the effects of wind waves.

In certain regions, wave set-up and particularly wave run-up can contribute significantly to water levels and increase the coastal flood hazard (Barnard et al., 2014, Vitousek et al., 2017b). These processes can become important where the shoreline is gently sloping and intense storm waves occur. Explicitly modeling waves is computationally intensive; however, there is extensive engineering literature that allows users to project hazards based on both wave properties at the coast and the shape and type of the shoreline (Stockdon et al., 2006, Eurotop II, 2018, U.S. Army Corps of Engineers, 1995). These formulas can estimate relative inundation hazard due to waves along varying shoreline types and exposures without explicitly modeling wave evolution in the nearshore. To use these equations effectively a good estimate of coastal elevation is essential. When available, a high-resolution digital elevation model (DEM) can be used to help estimate and constrain uncertainty of slope along shorelines.

This study evaluates coastal flood hazards around Long Island and Long Island Sound, NY, by combining existing publicly available datasets of historical observations with results from climate model projections and regional wave models to evaluate the regional variability in coastal flooding hazard now and in the future. The work is organized as follows: Section 2 describes the region, datasets and methodology, Section 3 provides results, Section 4 presents discussion of model output and coastal flood hazard in the study area, and Section 5 summarizes and concludes the work.

2.0 Methods

2.1 Study Area

The study area includes Long Island, New York, and the coastal watersheds of Long Island Sound and is shown as dark grey in Figure 1. The shape of Long Island Sound has led to spatial variability in maximum water levels during storms, the narrowing of the sound from east to west causes "funneling", a dynamic observed in other estuaries (e.g., San Francisco Bay, Nederhoff et al., 2021). This study area includes a small watershed in coastal Rhode Island, coastal Connecticut north of Long Island Sound and New York State's Westchester (coastal part), Bronx, New York

(Manhattan), and Kings (Brooklyn), Queens, Nassau, and Suffolk Counties on Long Island, NY. In our analysis, the domain is split into regions to investigate the spatial variability in coastal flooding from non-tidal residual water levels (storm surge) and storm induced waves. Figure 1 shows these regions: areas of the City of New York including Hudson River and the East River are in green, south shore of Long Island is in gold, Peconic Bay is in blue, north shore of Long Island is in pink, north boundary of Long Island Sound is outlined in black with the western part of this coastline in cyan, and the eastern part of this coastline in yellow. Some defined areas are overlapping, for example the northern shore of Long Island (black section) is also used in the western (cyan) and eastern (red) parts of Long Island Sound.

One reason for analyzing geographic regions separately is that the study area includes a range of shoreline types that can substantially affect spatial variability in coastal flooding. Much of the south shore of Long Island is characterized by barrier islands with marsh islands between the sandy barrier islands and the mainland. The more urbanized parts of this shoreline are heavily protected by bulk heads and sea walls, particularly on the more developed western side (purple line Figure 1). The amount of natural shoreline increases eastward along Long Island, where there is more agriculture and lower density development. The north shore of Long Island has predominantly natural shorelines, most of which are steep cliffs and bluffs (red line Figure 1). The shoreline in western New York and Connecticut along the northern shore of Long Island Sound is heterogeneous with various natural and man-made shorelines (black line Figure 1).

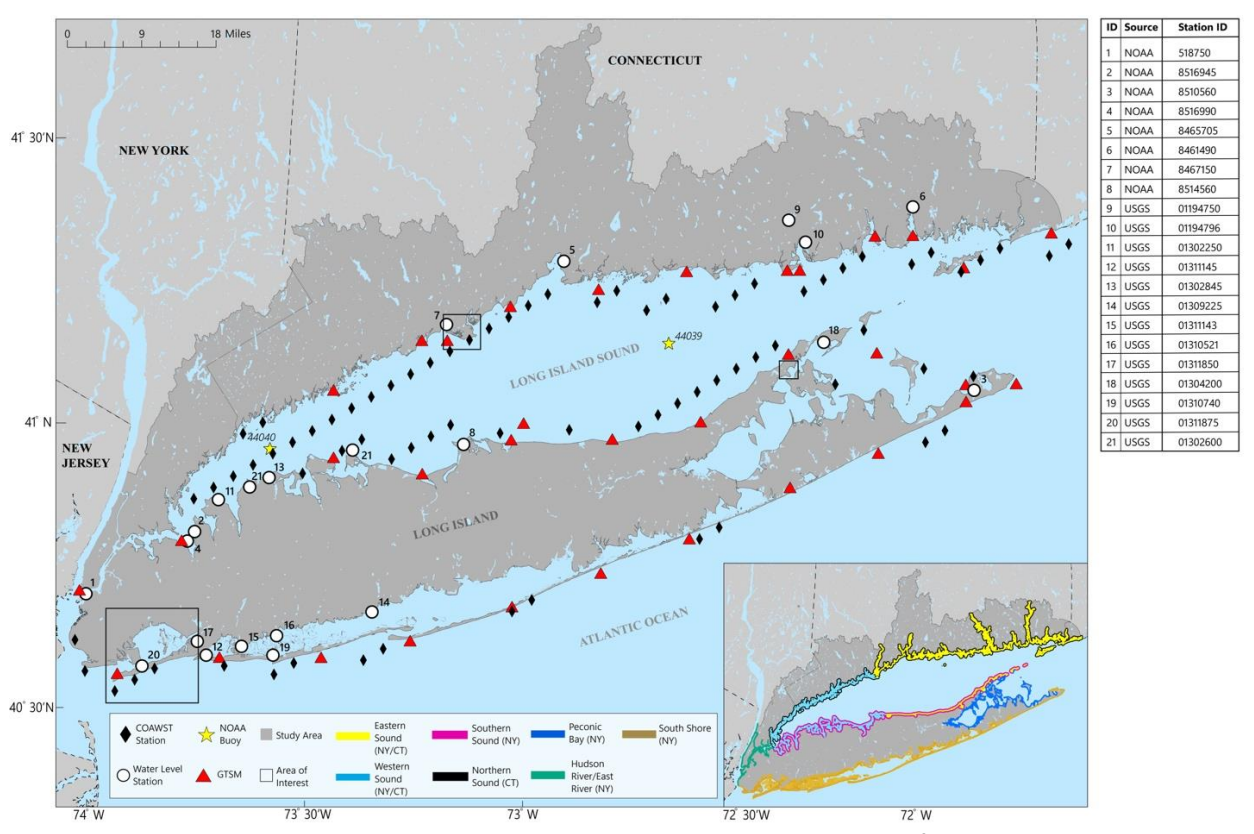


Figure 1: Study domain including Long Island, New York, and coastal watersheds of Long Island Sound. Domain is split into sections: New York City including Hudson River and East River (green), south shore of Long Island (gold), Peconic Bay (blue), north shore of Long Island (pink), north boundary of Long Island Sound (black outline), western part of Long Island Sound (cyan), and the eastern part of Long Island Sound (yellow). Water Level Stations, Global Tide and Surge Model (GTSM) and Coupled Ocean-Atmosphere-Wave-Sediment Transport Model (COAWST) output locations and National Oceanic and Atmospheric Administration (NOAA) buoys are also shown on the plot (refer to legend for symbols). Additional Information about NOAA sites is provided in Table 1. Base map from U.S. Geological Survey National Atlas digital data, 1:1,000,000 scale

2.2 Extreme Value Analysis (EVA) Methodology

Extreme value analysis (EVA) (Coles, 2001) was used to assign annual exceedance probabilities to extreme events from the daily time series of non-tidal residuals (NTRs) (storm surge) for current (Section 2.3) and future (Section 2.4) conditions across the study area as well as significant wave heights (Section 2.5). This approach assumes a distribution of extreme events that are 1) independent and 2) identically distributed (stationary in time). Generally, the time series for both water levels and wave heights used in this study were subsampled to a daily time step, and peaks were extracted using a peaks-over-threshold (POT) approach using a 95% threshold and a 3-day minimum between peaks to ensure independence. For water levels, the time series was first detrended to remove sea level rise which removes one of the potential causes of non-stationarity. There is good evidence that the effects of climate over the observational period have not increased the frequency of storms (Vecchi et al., 2021). Additional limitations caused by the assumption of identical distribution due to the mixing of storm types is discussed more in Section

4.2. The selected peak values were fit to a generalized Pareto distribution (GPD) for each location. The data and their corresponding fits were all evaluated with the Anderson-Darling test (Okabe et al., 2000) to confirm the data were consistent with the specified GPD fit. The GPD for each location was used to estimate the magnitude of storm surge or significant wave height associated with the annual exceedance probabilities (AEP) for 1, 4, 10, and 99 percent, which correspond to the 100, 25, 10, and 1-year recurrence interval or return period, respectively. The Anderson-Darling test was used to confirm the goodness of fit of the GPD to the time series (Gilbert, 1986). Mean flood extents for each AEP water level were calculated by adding mean higher high water (MHHW) for each station to the NTR for the given AEP scenario. This represents a condition where the peak NTR occurred simultaneously with a higher high tide.

2.3 Water Level Hazard

Observed Water Levels - Historical

Shown in Figure 1 and listed in Table 1, there exist 8 NOAA stations (NOAA, 2025) with recorded hourly water levels (in meters, referenced to the North American Vertical Datum of 1988, or NAVD 88) and 13 U.S. Geological Survey (USGS) stations (U.S. Geological Survey, 2025) with recorded 15-minute water levels (converted to meters above NAVD 88). Included time series had record lengths with approved data of at least 10 years. Although longer record lengths lead to better constraints on recurrence intervals, a minimum record length of 10 years was selected in alignment with the USGS guidance in estimating stream flood frequencies, (England et al., 2018). In this study, we chose to estimate flood hazard using the non-tidal residual (NTR), which is defined as the difference between observed water levels and predicted tidal water levels (NTR) (Pugh 1987). For stations where tidal water level predictions were not provided by NOAA, the Utide Python package was used to generate predicted tidal water levels (Codiga 2011). The resulting NTR time series was subsampled to daily maximum values, and the daily values were used in the extreme value analysis (Section 2.2).

<u>Modeled Water Levels – Historical and Future</u>

Modeled 10-minute total water levels were analyzed from a set of historical (1950-2014) and future (2015-2050) simulations of the Deltares Global Tide and Surge Model (GTSM; v3.0), a depth averaged hydrodynamic model that dynamically simulates the tides, storm surge and sea level rise (SLR) with a coastal resolution of 2.5 km (Muis et al., 2020, Muis et al., 2022a, Muis et al., 2022b). The historical simulated storm surge was modeled by forcing 10-meter wind speed and surface pressure from five general circulation models (GCMs) of the Coupled Model Intercomparison Project Phase 6 (CMIP6) climate projections from the High-Resolution Model Intercomparison Project (HighResMIP) multi-model ensemble (Haarsma et al., 2016). The GCMs consist of two atmosphere-only sea-surface-temperature (SST) forced simulations (HadGEM3-GC31-HM-SST (Roberts, 2017a) and GFDL-CMC192-SST (Zhao et al., 2018)), and three atmosphere-ocean coupled simulations (ECEarth3P-HR (EC-Earth Consortium (EC-Earth), 2018), CMCC-CM2-VHR4 (Scoccimarro et al., 2017), and HadGEM3-GC31-HM (Roberts, 2017b)). The

future storm surge simulations used the same GCMs but were based on the high-emissions scenario SSP5-8.5 (Shared Socioeconomic Pathways) (O'Neill et al., 2016). The most appropriate climate model simulation used for the future water level inundation analysis was determined by comparing projected surge level changes from the global sea level change indicators (Muis et al., 2022a). Of the five GCM model simulations, the CMCC-CM2-VHR4 was selected because it had the highest spatial resolution. One station within the domain was removed (GTSM station 15159) due to anomalously high increases which may be due to coarse resolution of the grid when compared to coastal features like nearby barrier islands. The NTRs are an available data product (Muis et al., 2022b), and these 10-minute NTRs were processed identically to the observed NTRs by finding a daily maximum, using peaks over threshold sampling at the 95th percentile threshold, and ffitting those peaks to a GPD to estimate an NTR for a given AEP. GTSM station locations are shown in Figure 1 and listed in Appendix 5.

Water Level Maps

The study area was divided into the Voronoi polygons (Okabe et al 2000) surrounding each water level station. At each water level observation location, the water level for a given AEP was projected onto the digital elevation model (DEM) using the Simulate Water Level Rise/ Flooding tool in Global Mapper (Blue Marble Geographics, 2024), version 25). This algorithm floods the terrain below the given depth if there is a path for the water to arrive at the low elevation area. The flood extents were cut off at the Voronoi polygon edge and merged to create a flood extent over the entire study area for that AEP; where any small overlaps existed, the higher water level was selected. The terrain for this analysis was derived from a mosaic of a 1-meter DEM and a 0.7-meter DEM (Danielson et al., 2016) that together were able to cover the study area.

Water Level Hazard Ranking

The study area shown in Figure 1 was subdivided into 11,407 900-meter by 900-meter grid cells for the purpose of integrating the spatial datasets to calculate and map the coastal water level flood hazard. For each annual exceedance probability (AEP) scenario (1, 4, 10, and 99 percent) the percent of inundated land within the grid cell was computed. The kmeans clustering algorithm in the scikit-learn Python library (Pedregosa et al., 2011) was used to find the natural breaks in the flooding distribution and assign rankings from 1 to 5. More details are discussed in Appendix 4. The final water level hazard ranking and all inundation extents are available as shapefiles in Cook and Herdman (2025).

2.4 Wave Hazard

Estimating wave hazards is difficult due to the highly random nature of waves and the high spatial and temporal variability in shoreline slope and type (structure versus natural) along coastal regions like Long Island and Long Island Sound. Therefore, this study uses wave overtopping and the associated discharge volume as a metric to describe the spatial variability of wave

interactions with the shorelines across the study area. Wave overtopping is the time averaged amount of water that is discharged (liters per second) per length of a structure (meters). This process depends on the significant wave height, H_s (Section 2.4.1), and the vertical crest of the coastal structure, R_c (Section 2.4.2), and is highly stochastic in nature. In other words, not all waves will lead to overtopping, and the extreme storm waves that lead to overtopping do not continuously discharge water over the structure. This quantity is usually only applied to engineered structures, but in this study, it is used as a metric to quantify the strength of wave interaction with the shoreline. Again, this study does not provide specific estimates of overtopping discharge but rather estimates a relative flood hazard by estimating a quantity that should correlate to the order of magnitude of flood hazard as it pertains to volume of water for a given wave event (Section 2.4.3).

The following equation was used to estimate wave overtopping and is based on the general formula from Owen (1980) and described in Eurotop II, (2018),

$$\frac{q}{\sqrt{gH_s^3}} = 0.1035 \cdot \exp\left[-(1.35 \frac{R_c}{H_s \cdot \gamma_f \cdot \gamma_\beta \cdot \gamma^*})^{1.3}\right] \tag{1}$$

where q is the mean overtopping discharge (*liter per second per meter*), g is the acceleration due to gravity (*meters-second*-2), H_s is the incident wave height, R_c is the crest freeboard, γ_f is the influence factor for roughness elements on a slope, γ_{β} is the influence factor for oblique wave attack, and γ^* is a combined influence factor for a storm wall on a slope or promenade. When an influence is not present, the influence factor becomes 1.0. If a certain influence is present, the value of the influence factor becomes smaller than 1.0 and the wave runup and wave overtopping discharge will decrease. Assessing the influences across the study area was beyond the scope of the project; therefore, we assumed the worst-case scenario and applied the maximum influence factor of 1.0 across the domain. More detailed engineering studies of coastal dynamics and structures are needed to better approximate wave overtopping at a localized scale. The following sections describe how wave height and crest freeboard were determined.

2.4.1 Significant Wave Height, H_s

Wave data within Long Island Sound and offshore are sparse and do not indicate the transfer of waves from the nearshore to the coast. Significant wave heights are extracted from the Coupled Ocean Atmosphere Wave and Sediment Transport (COAWST) forecast modeling dataset (Warner, 2022). Significant wave height is defined as four times the standard deviation of the surface elevation. A total of 83 COAWST stations (shown in Figure 1) within the domain covered approximately 9 years from 2011 through 2019. We compare the significant wave height from NOAA NDBC buoys 44039 and 44040 (gold stars in Figure 1) with the closest COAWST stations (time series in Appendix 1, Figure A1). Cumulative distribution functions of the comparison are

shown in Figure 2. COAWST captures the distribution of the wind speeds, especially between 15-25 m/s, but fails to capture the extremely high values, > 25 m/s. While the model generally slightly underpredicts winds, this bias is the same at both buoys indicating that the gradients that we see in wave energy along the axis of Long Island Sound are real. This bias towards slower winds could underpredict waves and therefore discharge values for the highest wind-wave events. Ilia et al. (2023) reported that in western Long Island Sound, the top 10% of their modeled wind speeds were lower than observed values because of the coarseness of the gridded wind model used as a model input. They used correction factors for wind forcing in western Long Island Sound and improved their wave estimates. Because we are using published model outputs from the COAWST forecast, we are unable to make this modification.

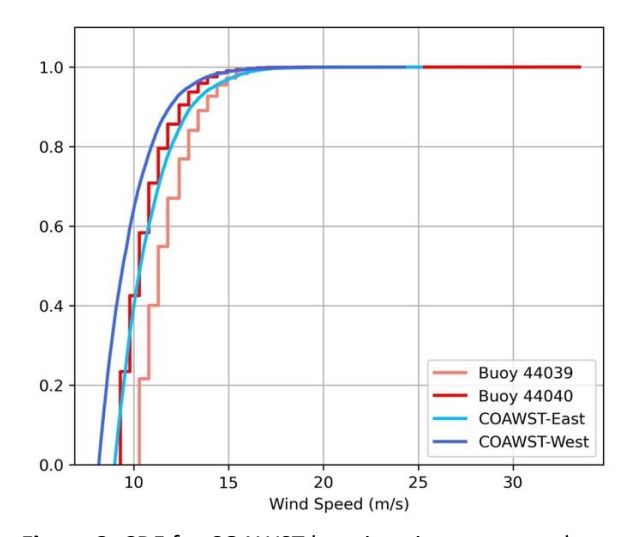


Figure 2: CDF for COAWST locations in eastern and western LIS compared with NDBC Buoys 44039 and 44040.

Using the modeled significant wave heights described above, we apply the Extreme Value Analysis approach (Section 2.1) like the NTR (Section 2.2). We identify daily max values of wave height, find the POT (95%, 3-day between events) and fit those peaks to a GPD, and calculate the same range of AEP scenarios (1, 4, 10, and 99 percent) for significant wave heights as we did for NTR (storm surge).

2.4.2 Crest Freeboard, Rc

The crest freeboard is extracted from the Continually Updated Shoreline Product (CUSP; National Geodetic Survey (NGS), 2023) and the 1-meter DEM. Using the ArcGIS Pro Data Management geoprocessing tool Generate Transects Along Lines (Esri, 2024), 100-meter transects were calculated every 100 meters along the CUSP shoreline (Figure 3, left panel). Elevations (referenced to NAVD 88) along each shore-perpendicular transect were extracted from the 1-meter DEM of the domain. A 4-meter rolling average was applied to smooth the transect, and the first peak shoreward of mean high water (MHW) was identified as the crest location. The vertical distance between this value and MHW was defined as the crest freeboard (Figure 3, right panel).

If the shape of the transect was such that no peaks above MHW were identified, no freeboard was identified, and the transect was not included in the computations.

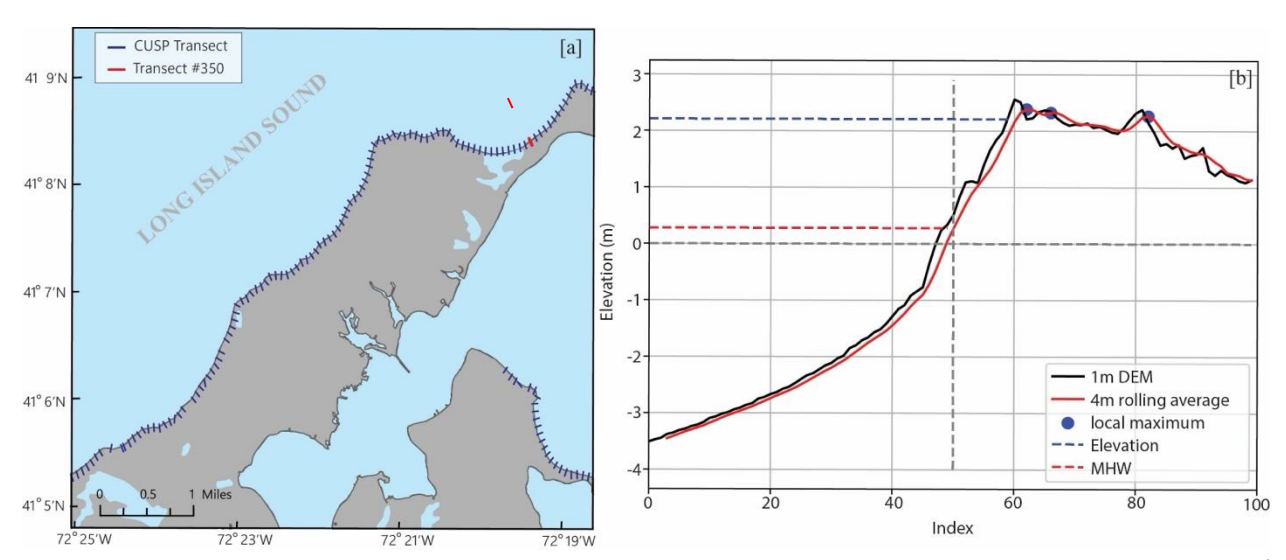


Figure 3: 100-meter transects every 100 meters along CUSP dataset along the Long Island Sound shores north of Greenport, NY [left panel]. An example of a transect [right panel], location shown as the red transect in the left panel.

2.4.3 Wave Hazard

The wave hazard ranking was based upon the discharge thresholds identified in Eurotop II (2018) that differentiate base on order of magnitude of hazard. The median value of the discharges in each 900-m grid cell from the different scenarios considered was used to assign the wave ranking in each cell. The following ranges of discharge correspond to sequentially increasing rankings (1-5); less than 0.1 L/s, 0.1 to 1 L/s, 1 to 10 L/s, 10 to 100 L/s, greater than 100 L/s. These break points were set based on the associated hazard potential with increasing orders of magnitude of wave discharge and resulted in relatively high wave hazards throughout the study area. The final wave hazard ranking is shown in Appendix 4, Figure A4b and in Cook and Herdman (2025).

3 Results

3.1 Statistical model of the observed non-tidal residual (NTR)

The NTR time series from the 21 stations (white circles in Figure 1) were successfully fit to a general pareto distribution (GPD). The data and their corresponding fits were all evaluated with the Anderson-Darling test. An example of a GPD fit is shown in the middle panel of Figure 4 for The Battery, NY (NOAA station 8518750; NOAA, 2025); all other stations are shown in Appendix 2. All the observational points were within the confidence intervals of the GPD model, and the fit was virtually identical to the observations for the smaller more frequently observed storm surges. Across all NTR time series, the POT method identified an average of 10.7 storms per year (Table

1). The largest observed non-tidal residual at the Battery, NY, (Figure 4a) occurred during Post-Tropical Storm Sandy in October of 2012 and was larger than what the statistical model indicates for the 100-year event (Figure 4b). In fact, across all water level stations, Sandy was the largest deviation from the GPD fit, shown as the circled plus signs in Figure 5c. Outside of Sandy, the average deviation from the GPD fit was ±20 cm (Figure 5c). This large difference between an empirical estimation of return period from the data and the return period from the GPD fit (apart from the Battery) is primarily due to shorter duration observational records that included Sandy. This is because the empirical return period, by definition, is restricted to be at or below the length of the observational record. Thus, the same large storm, e.g., Sandy is an almost 100-year event at the Battery (where there is a long record) but is a 15-year event at a station with a shorter record.

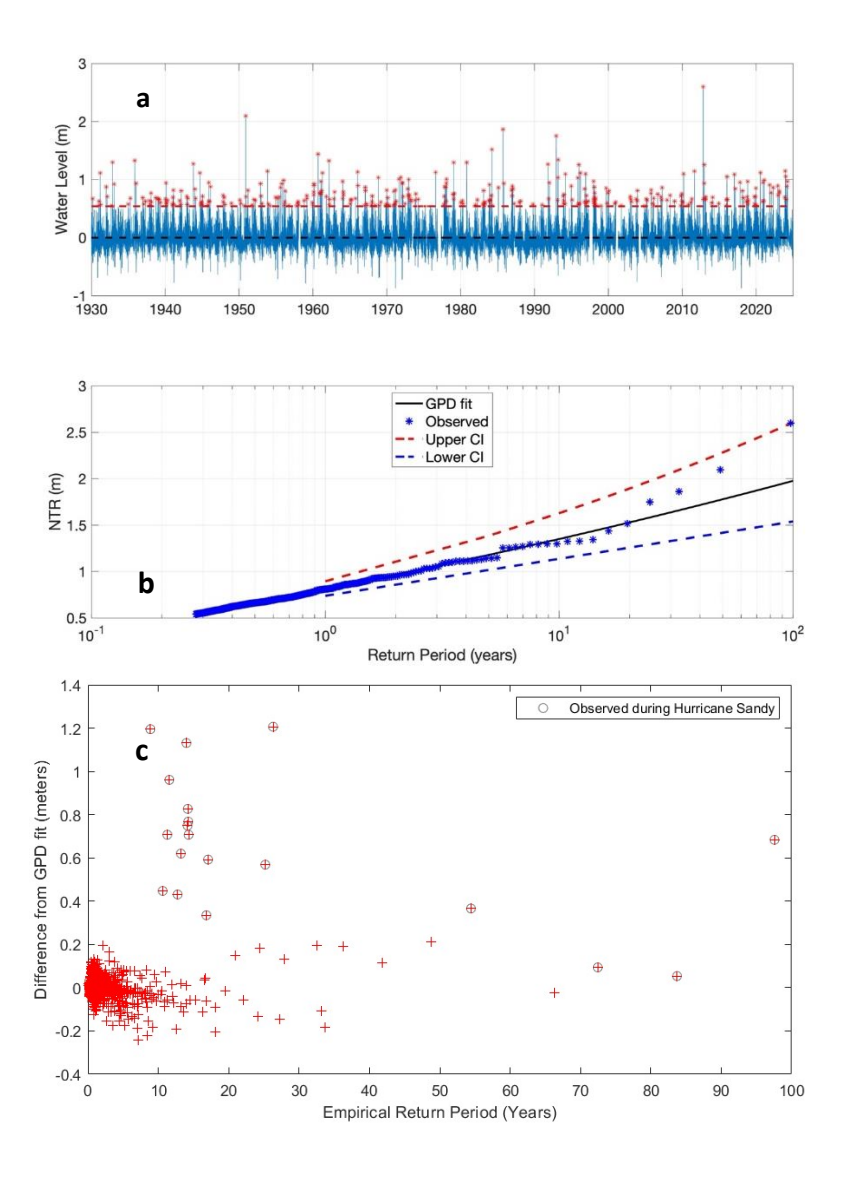


Figure 4. NTR filtered time series for the Battery, NY (NOAA: 8518750, white circle in Figure 1 in Manhattan, NY) with peaks over 95% threshold (red asterisks) with a 3-day minimum gap between peaks [top panel]. Example of

GPD fit to the observed water levels at the Battery, NY (NOAA station 8518750) with confidence intervals (CI) [middle panel]. Differences from empirically fit return periods and predicted non-tidal residual water levels from a GPD fit across all stations for different return period values, with hurricane Sandy points circled [bottom panel].

Many of the largest events in this region are associated with hurricanes. Of the top 5 coastal inundation events across all 21 water level stations (105 events) roughly 47% were due to nor'easters (extra-tropical cyclones), 19% were due to snowstorms/blizzards, and 34% were due to hurricanes (tropical cyclones). The top four events in the NTR time series of water level peaks were Superstorm Sandy (19 events), the 2012 nor'easter (14 events), 2017 bomb cyclone (10 events), and Hurricane Irene (9 events). The next highest cluster of events were all nor'easters from 4 different events (1984, 1950, 2010, 2024). The GPD fit does a reasonable job of capturing the frequency of these water levels even though they are caused by different physical drivers. Again, the largest exceptions are associated with Sandy, particularly during record lengths of about 15 years usually associated with USGS gages (Table 1). Further discussion on storm type is included in Section 4.2.

3.2 Statistical model and future analysis of the GTSM-GCM modeled time series

The same EVA methodology was run on 34 GTSM modeled historical and future NTR time series (locations in Figure 1). Again, all the GPD fits to the GTSM modeled time series within the domain pass the Anderson-Darling Test at the 5% significance level. First, we compare an empirical distribution with a GPD fit to the observed NTR (Figure 5; left panel) and find that in general, the comparison follows the 1:1 line and there is higher spread at higher NTRs (or higher AEP). We then compare the GPD fit to the observed NTR with the GPD fit to the GTSM GCM modeled future NTR. The GPD fit to the model is from the stations located closest to the observational gages (Figure 5; right panel). The GCM forced GTSM model shown in the right panel of Figure 5 is the CMCC-CM2-VHR4 model (Scoccimarro et al., 2017).

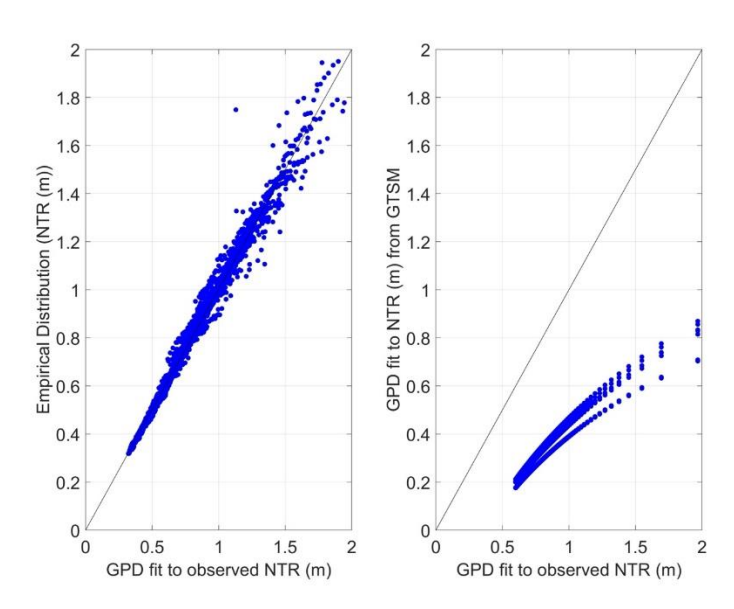


Figure 5: A comparison of NTRs between empirical distribution and GPD fit to observed daily max of NTR [left panel] and GPD fit to observed NTR time series and corresponding GTSM filtered NTR time series for the CMCC model [right panel].

Overall, the water level predicted from the GPD fit to the observed NTRs was larger in magnitude and showed more variability between stations than the equivalent water levels from the GPD fits to the GTSM GCM modeled NTRs (Figure 6, right panel). Because the GPD fit to the observed NTR more closely matched the empirical distribution (Figure 6, left panel), and to prevent underpredicting coastal inundation, we chose not to use the values from the future GTSM NTR time series. Instead, we found the absolute change from the historical to future modeled GTSM (CMCC-CM2-VH4) NTR and added that quantity to the observed NTR time series to compute our future NTR projections across the domain.

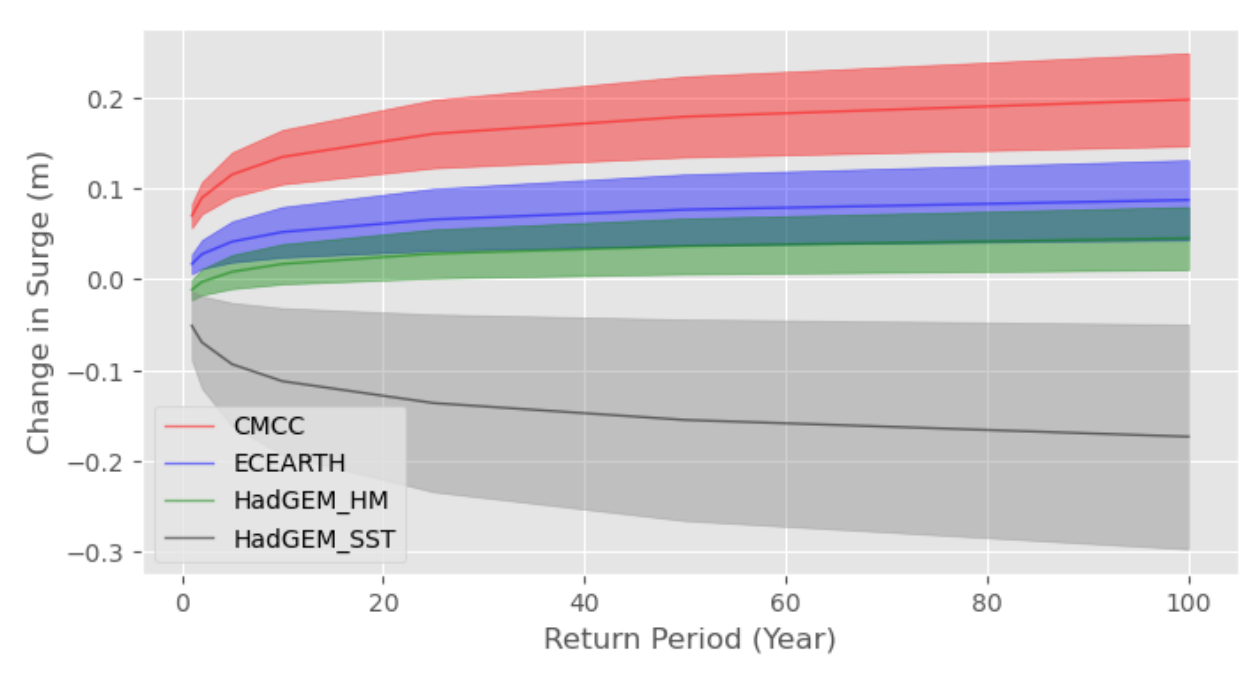


Figure 6: Regional analysis of change in storm surge for different GTSM models. Lines show average change in storm surge between historical epoch (1985-2014) and future (2021-2050) for all GTSM stations shown in Figure 1, with shading indicating one standard deviation.

The change in NTR associated with a given AEP due to climate change from the model is shown in Figure 6. For each GCM, the background sea level rise was the same, so the only difference in the projected changes is due to storm activity. Of the 5 GCM options available (refer to Section 2.3), the CMCC-CM2-VHR4 model was chosen because it had the highest horizontal resolution in forcing and showed the largest change in NTR, representing the most conservative future estimate of storm changes to water levels. The regional average for CMCC-CM2-VH4 indicates the annual storm is expected to increase NTR between 4 and 9 cm in this region, while the 100-year storm is expected to increase between 10 and 29 cm in the region. There is no clear geographic pattern in this increase, and some of the spread appears to be related to the coarse

bathymetry of the GTSM model in our study region, so we applied the average increase to all observation stations to best represent the predicted changes. Because these simulations include both sea level rise and future climate projections, the change in NTR from the GTSM models should both represent the change in storm intensity (as resolved by the climate models) and any non-linear interactions with the increasing water depth.

3.3 NTR coastal inundation Maps

The coastal inundation extent for each current-day AEP from the NTR time series analysis across the domain is shown in Figure 7 (top panel) with insets shown in Figure 8 (top panels) and in Cook and Herdman (2025). In general, inundation of areas near the coast or large rivers is expected. As a validation of our methodology, we compared our inundation extents from the 0.01 AEP current scenario to the inundation extent predicted by FEMA (Appendix 3). The inundation extent for the future cases, where NTR is increased by the amounts shown in Figure 6 and described in Section 3.2, is shown in Figure 7 (bottom panel). There are a few locations in the region where the area inundated significantly increases as the magnitude of the event increases (the frequency of the event correspondingly decreases). Some of these locations are shown in the insets of Figure 8, where the top panels are current AEPs, and bottom panels are future AEPs. Areas that are characterized by relatively low-lying land show large changes in inundation extent, such as Jamaica Bay, NY shown in the middle panes of Figure 8.

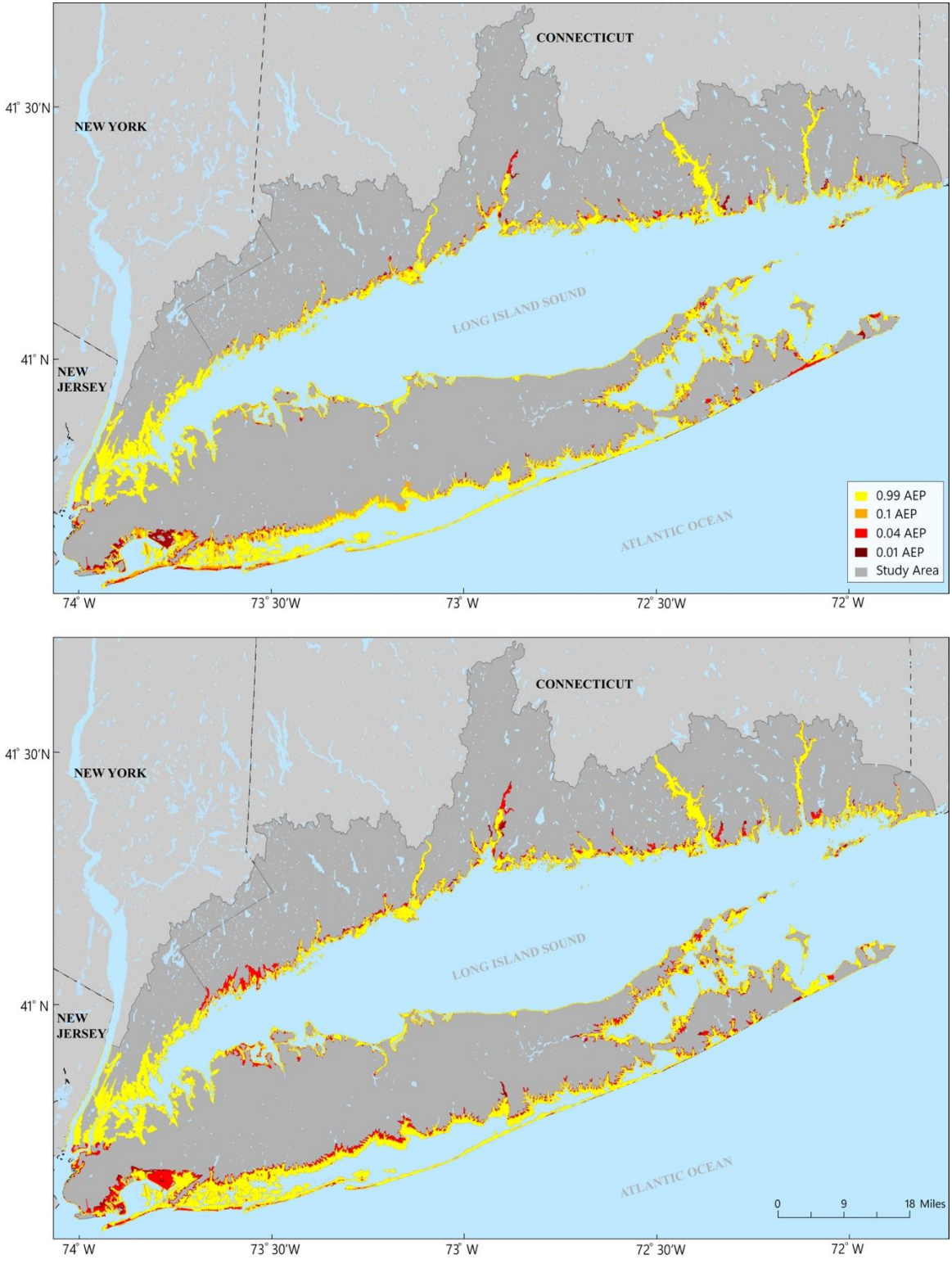


Figure 7: Water level inundation extent across the entire domain for current water levels (top) and future water levels (bottom).

The future inundation extent changes due to the projected increases in NTR water level for each given AEP. However, the broad patterns of flooding are not significantly different in the future. Low lying areas along the coast and rivers are still the locations most susceptible to flooding. However, the size of the area flooded, and the corresponding frequency of flooding is increased substantially in many locations. We observe substantial increases in flooded area along the south shore of Long Island, particularly in and around Jamaica Bay (Figure 8, middle panels) and the west end of Long Island Sound. Additionally, areas along the shores of the Peconic estuary and the north fork of Long Island (Figure 8, left panels) show flooding. The inundation extends farther upstream in most of the tributaries, which is particularly noticeable along the rivers in Connecticut (northern Long Island Sound). Particularly along river channels flooding may be different than what is shown here because this study is limited by the exclusion of river discharge, which was not the focus of this study. The shifts in inundation extents and frequency from current conditions into the future are highly spatially variable, but generally areas that show flooding with some frequency under current conditions show a more frequent inundation frequency in the future. In the inset comparing a location near Greenport, NY (Figure 8a) there are areas where in projected future conditions, the annual flood potential has a similar extent to the 0.01 AEP current inundation extent. (Figure 8 left panels). This represents a factor of 100 increase in flooding frequency for those areas, which would be substantial change.

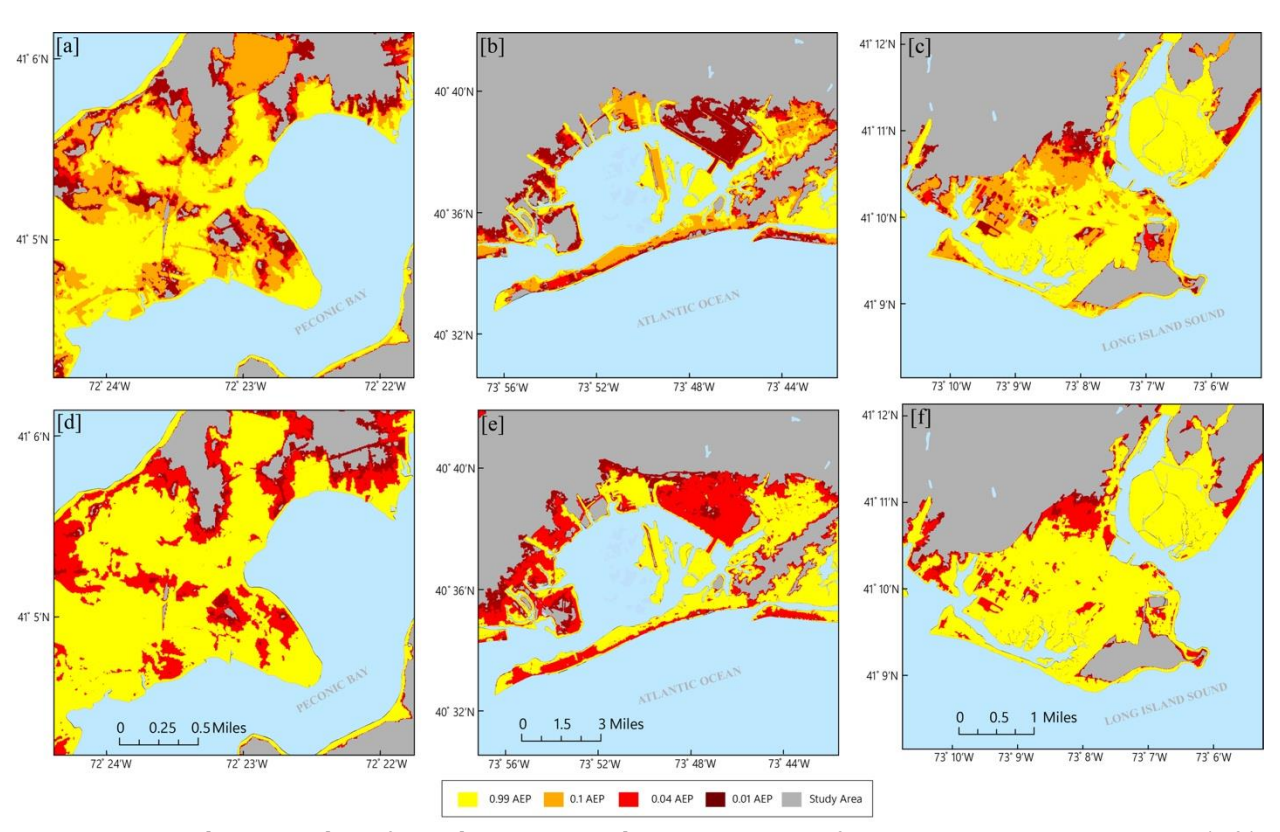


Figure 8: Current [top panels] and future [bottom panels] inundation extent for three locations: Greenport, NY (left), Jamaica Bay, NY (middle) and Bridgeport, CT (right).

3.4 Wave Results

The wave hazard depends on the wave energy reaching the shore as well as the shape and elevation of the shoreline. Figure 9 shows the shoreline elevation (top panel), wave height for the 0.01 AEP (100-yr storm) (middle panel), and the associated wave hazard metric, wave overtopping (discharge) (bottom panel). Wave heights ranged from 2.3 m to 11.1 m. The wave hazard is highest along the southern shore of Long Island where there is the greatest wave energy (Figure 9, middle panel) and the relatively low elevation barrier islands and sandy beaches (Figure 9, lower panel). The lowest wave hazards occur on the west end of Long Island Sound, where the more protected shoreline is subjected to less wave energy, and the northern shore of Long Island which is characterized by very steep topography with many cliffs. The locations with higher wave hazards in Long Island Sound are generally locations where the shoreline elevation is lower which primarily corresponds with beaches and marshlands. Ninety-one percent of the shoreline that is impacted by the 0.01 AEP (100-yr) storm is also affected by wave hazards in the highest category, which indicates significant wave overtopping and strong potential for erosion if not protected by some sort of armoring.

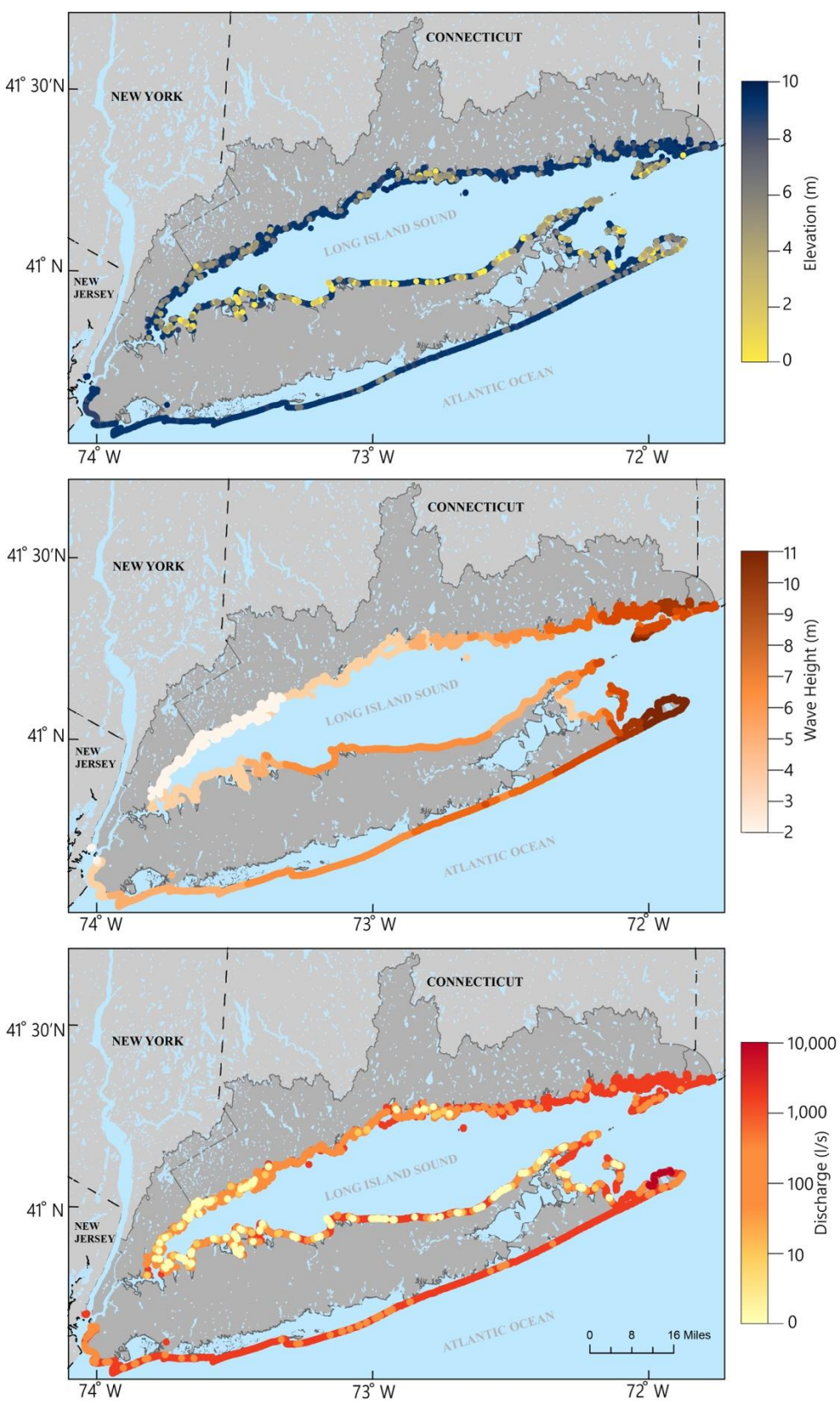


Figure 9: Elevation above NAVD 88 from DEM (top panel), 0.01 AEP (100-yr return period) for wave height (middle panel), and Discharge for 0.01 AEP (100-yr return period) (bottom panel).

There is spatial variability in the length of shoreline impacted by large wave overtopping (discharge) in the different AEP scenarios (Figure 10). In western Long Island Sound, the length of shoreline experiencing the highest classification of wave hazard does not change significantly between the different frequency wave events (Figure 10). The equation (Eq. 1) used to assess wave hazard has an exponential dependence on the ratio of the shoreline height to the wave height. The range of conditions that lead to large wave hazards ranges from lower wave heights (1 m) that are equal to the shoreline elevation, while larger wave conditions (8 m) can be only half the magnitude of the shoreline elevation. In locations where there is not a significant difference between the 0.99 AEP and the 0.01 AEP, this indicates that even the larger waves stay below the threshold of approximately half of the shoreline elevation. However, in eastern Long Island Sound and along the north shore of Long Island, the length of shoreline that is impacted by potentially erosive wave hazards increase significantly with the more energetic (and rarer) wave conditions (lower AEP scenario). In these locations, the wave heights span a range that is closer in magnitude to the shoreline crest elevation, so significant increases in wave hazard occur as the wave height increases. The low wave energy and steep shorelines in and around the Hudson River prevent the wave hazard from becoming particularly large in most scenarios.

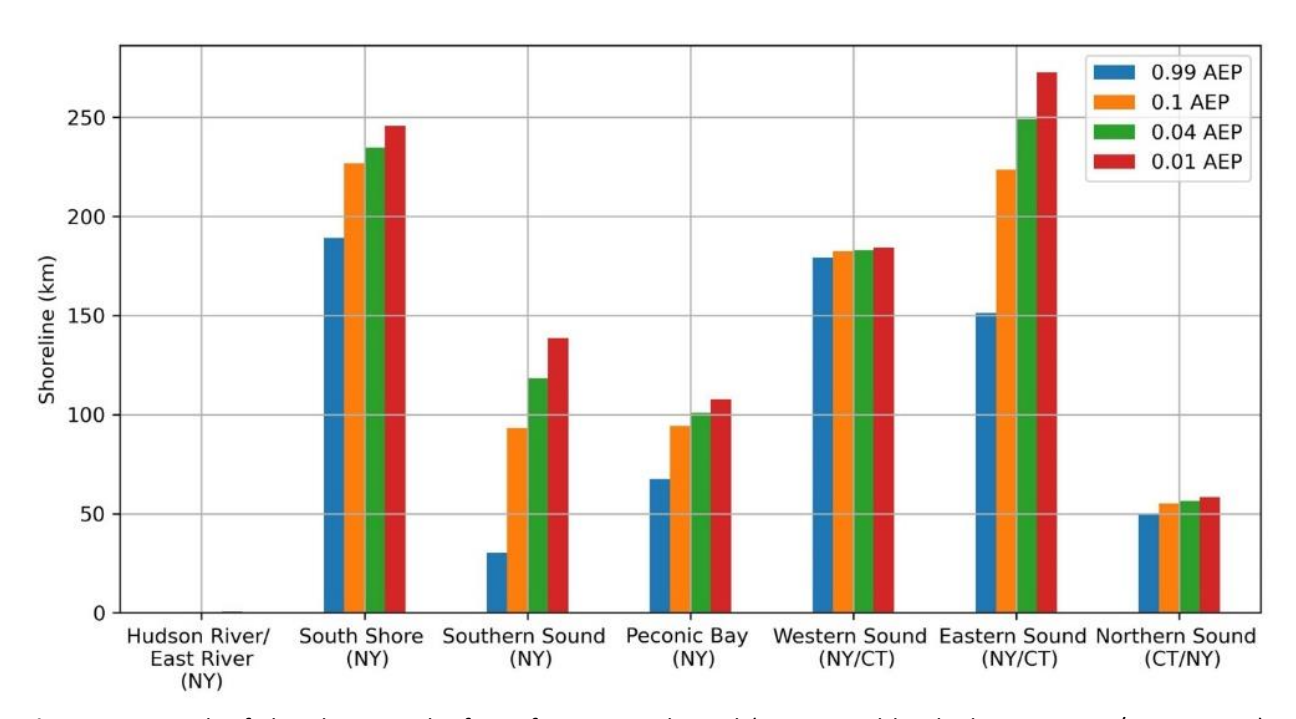


Figure 10: Length of shoreline at risk of significant wave hazard (categorized by discharge >100 L/s per meter), separated by region, colored by AEP.

4 Discussion

4.1 Regional Variability

Regional variability in coastal flooding can be due to geographic variability in physical characteristics like shoreline elevation and geology as well as environmental conditions like prevailing wind directions and storm wave heights. Understanding this variability can help managers allocate resources during extreme events and plan for future mitigation. Separating the AEP scenarios for NTR water levels for the regions described in Section 2.1, we can address the spatial variability across the domain. We have defined the water level hazard by the amount of land that is inundated; Figure 11 shows the area of land inundated by region (Figure 1) for the eight (current and future) AEP scenarios. The largest flooded areas are on the south shore of Long Island where there is extensive low-lying area (Figure 8, top panel). Along the Connecticut shoreline, the difference in flooding from west to east is driven by the low-lying land adjacent to the rivers (e.g., Connecticut River, Quinnipiac River, Thames River) in the area. Western Connecticut and Westchester County, NY do not have larger rivers and associated low-lying river valleys, so the coastal flooding is contained to areas that are near the coast (Figure 7). The relatively small area inundated on the southern shore of Long Island Sound is due to the steep cliffs that make up most of the coast in this area. The area around the Hudson River is adjacent to the most densely developed part of the study, New York City, and is characterized by relatively steep shorelines, with much of the area composed of man-made sea walls and structures. Area inundated is one way of evaluating the impact of a storm event; however, the cost associated with that event does not necessarily scale linearly with the area, as shown in (Nederhoff et al., 2024). Due to the highly developed areas that are inundated in the Hudson River area, this area could have the most economic impact when flooded despite being smallest in total area.

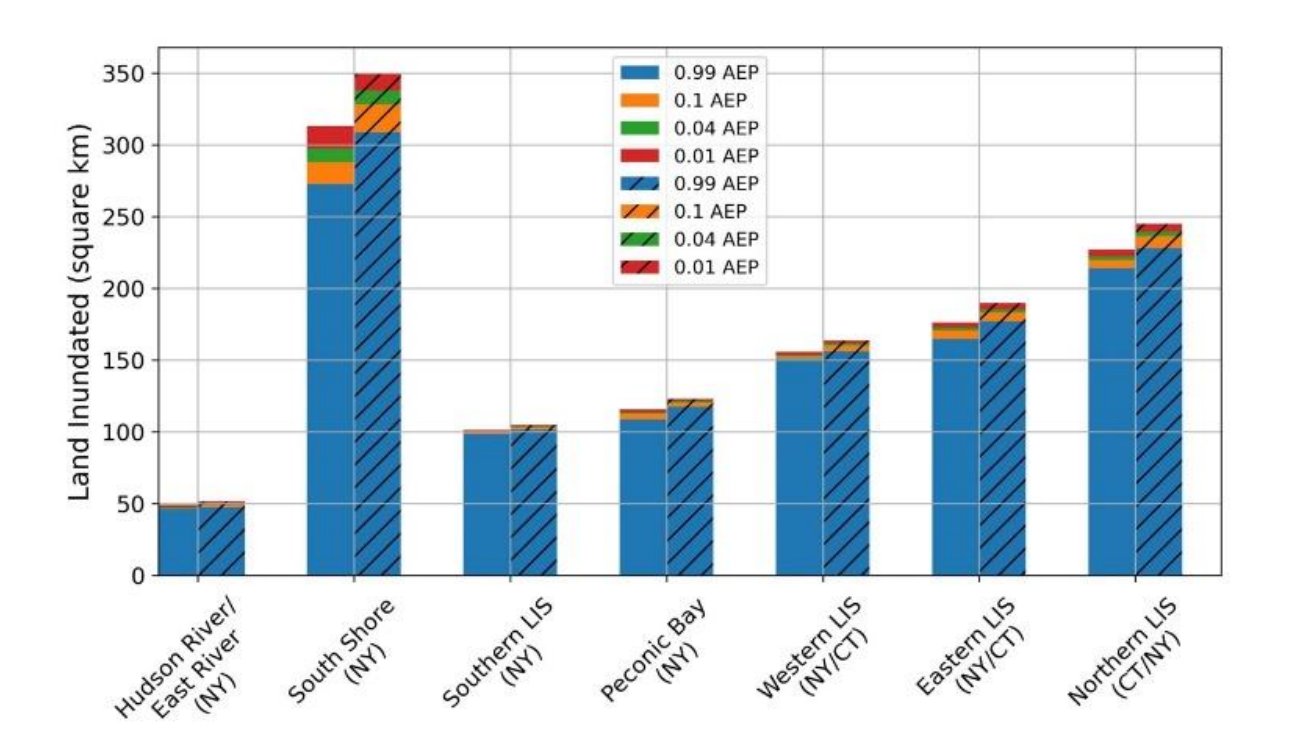


Figure 11: Area of land inundated by region colored by AEP. Hatched areas correspond to future AEP. Regions are shown in Figure 1.

Knowing how regional inundation patterns are changing can help inform future planning of land use and development. Figure 12 represents the percent change in area flooded in the future due to the increase in NTR and sea level rise. The change in the area flooded during a given event with an expected annual frequency ranges from 3 – 14% (y-axis, Figure 12). The largest increases in flood extent occur on the south shore of Long Island. The increases in future inundation of northern Long Island Sound are primarily driven by the increases along the eastern shoreline of Connecticut. The percent increase is not consistent across AEP with some locations showing the biggest jump for a one-year event (0.99 AEP) and some showing the largest jump for less frequent events. These small percentage increases may seem insignificant; however, along the south shore of Long Island, a 10% increase is an increase of 30 square kilometers of area inundated, which is more than 4,000 soccer fields.

In the Hudson River area, the 5% increases observed are close to 5 square kilometers of additional area, which is close to 700 soccer fields of inundation in densely populated Manhattan and surrounding areas. However, measured increases are averaged across the entire area, and there can be local hotspots that see a much larger increase in flooding frequency (such as those shown Figure 8). The associated shapefiles available in Cook and Herdman (2025) can be examined to evaluate local inundation more precisely. This increase in frequency of flooding in certain areas has real world consequences. For example, a zone with a 0.01 AEP (100-yr storm) for flooding changing to one with a 0.04 AEP (25-yr storm) for flooding represents a shift from a less than 30% chance of flooding over the course of a 30-year mortgage to an over 70% chance of flooding in that same time frame.

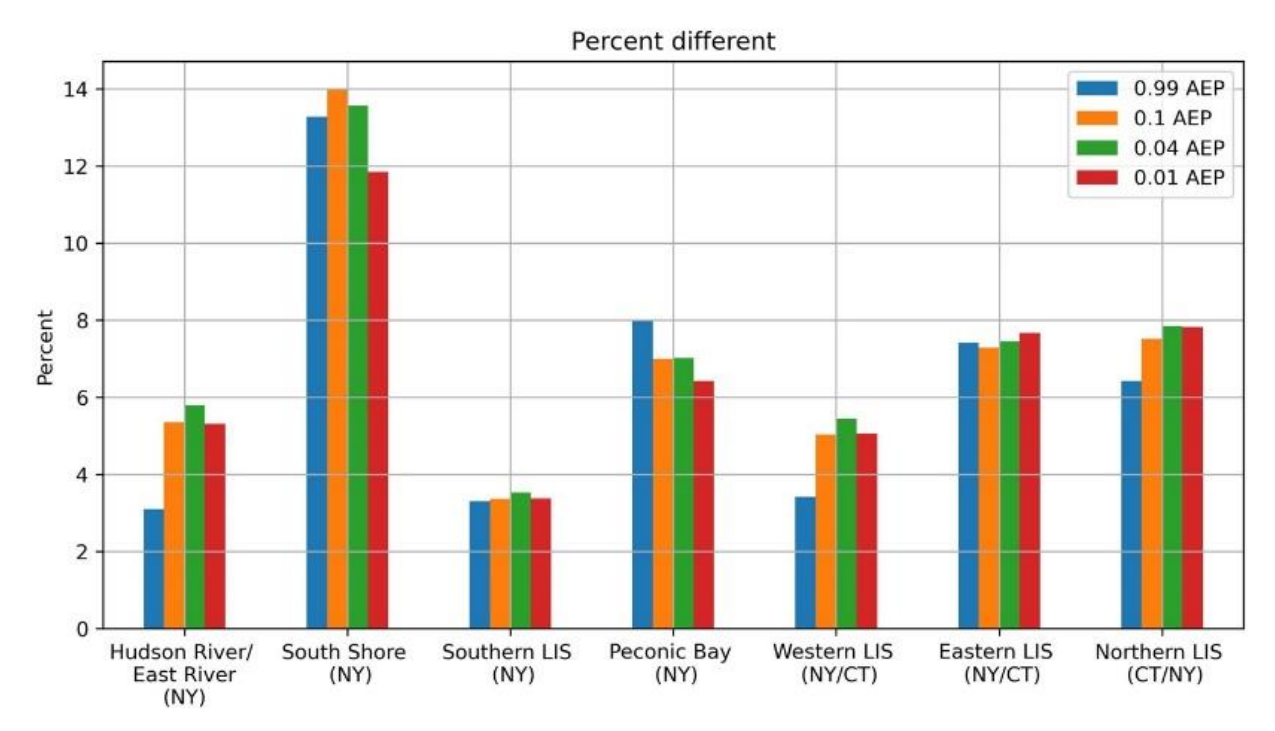


Figure 12: Percent difference in current and future land inundated separated by region, colored by AEP. ((future-current)/current)

4.2 Extreme Value Analysis (EVA) methodology

The GPD fit accurately captures the return periods for the observed NTR water levels at all the stations in the study area (Appendix 2, Figure A2a and A2b). However, the definition of NTR can provide some variability in the value of the residual water level and can lead to different interpretations of results. For example, the National Oceanic and Atmospheric Administration (NOAA) has performed an extreme water level analysis at all the NOAA stations in the study area with a sufficiently long record (NOAA, 2013). NOAA's methodology is different from the methods used in this study because it considers the total still water level, does not separate out the nontidal residual (storm surge) component, and uses annual maxima sampling, not peaks over threshold (POT). Because the planetary motions that drive tides are independent of the smallscale storms that create non-tidal residuals (storm surge), our methodology is a more conservative approach that considers the non-tidal residual as a separate independent variable and then adds the non-tidal residual back to the mean higher high water (MHHW) to assess the hazard for the highest total water level. Additionally, the annual maximum approach does not represent coastal water level datasets well because there is no physical reason that multiple large storm surges should be separated by equivalent time blocks. Using POT in place of annual maxima can improve the estimate by allowing for multiple large storms from one year to be included in the analysis.

Ultimately, these different methods do not provide substantially different results but allow for a sense of the uncertainty in the statistical modeling based on the sampling method used for selecting the extreme storm event. The estimates show here from the POT method are generally higher than but within the range of uncertainty of the NOAA estimates (NOAA,2013) of water level for a given return period. The one exception to this is that the method we used to estimate the one percent annual exceedance percentage NTR for Bridgeport, CT, resulted in an elevation of 2.54 meters compared to the 1.65 meters estimated by NOAA (both referenced to NAVD 88).

FEMA and NACCS have also evaluated the level of inundation associated with a 0.01 AEP in Long Island Sound. The comparison of inundation extents in our study with extents projected by FEMA and NACCES are provided in Appendix 3 (Figure A3). There are no significant differences despite the difference in methodologies. In the NACCS studies, the resolutions in and around Long Island Sound and Long Island were too coarse to accurately simulate water levels in regions with highly variable shorelines (Liu et al., 2020). Additionally, our study provides an analysis of the 0.01 AEP and more likely events, which can be important to consider when developing shoreline and drainage infrastructure.

4.3 Storm type

As previously mentioned, the biggest events in this study area are hurricanes or extra tropical cyclones. Our statistical model predicts lower water levels than those associated with the largest observed storms which tend to be hurricanes. One way to rectify this underprediction of water level associated with a particular storm types would be to divide the population of storms into different types and estimate water levels just associated with hurricanes. However, hurricanes do not occur frequently enough to have sufficient observations to create a statistical model so this option is not available. Despite this clear limitation, it is a widely applied method to fit a statistical model like the GPD to observed water levels or NTR data (regardless of storm type) to predict a frequency level associated with an extreme condition or storm event (NOAA,2013; Arnes et al, 2013; Sweet et al, 2020)

One limitation of the study is that the GTSM model does not explicitly resolve cyclones. However, the ability of global climate models to resolve extra tropical and tropical cyclones is improving with increased grid resolution. An analysis of the change in tropical cyclones in the North Atlantic in the highest resolution CMIP6 model indicates no change in storm frequency in our region of interest and small (if any) increases in storm intensity, as represented by wind speed (Roberts et al., 2020). The latest suite of models released as part of CMIP6 indicate that there will be fewer extra tropical cyclones (ETC) in a warming world, and these ETCs will also have slower propagation speeds throughout North America (Crawford et al., 2023). The impact of storm speed on storm surge level is highly dependent on the bathymetry of the shoreline. As such, the

impact of slower moving storms on coastal storm surge values is difficult to predict (Zhang & Li, 2019). Slower ETCs will likely mean larger amounts of precipitation accumulating over the land area for a given storm and this can have significant impacts on the potential for compound flooding.

5. Conclusion

We presented a statistical analysis of current and future coastal driven flood hazards on Long Island, NY, and the watersheds of Long Island Sound. A combination of observations and global climate model (GCM) projections were used to predict how storm induced coastal flooding may change in the future. An analysis of regional modeled wave conditions near the shoreline was included to better understand the magnitude and spatial variability of the potential wave hazard. This method utilizes publicly available datasets and inexpensive mechanistic modeling; therefore, this approach is a simple and low-resource way of assessing the varying regional coastal flooding hazards and wave event annual exceedance probabilities for a region, in this case Long Island, NY, and Long Island Sound. The reliance on existing data means this approach lacks the dynamic modeling that a process-based model would provide. Nonetheless, the EVA using the GPD fit provided an adequate fit to evaluate the NTR and wave time series, allowing examination of regional patterns in coastal flood hazards. While there are some hotspots of change, on average, the future 0.01 AEP (100-year) event shifts to become a 0.04 AEP (25-year) event. This increased frequency in flooding could substantially affect communities and critical infrastructure.

The current state of regional and global models limits understanding of future hazards. The GTSM model represents a major step forward in representing the interactions of surges with tides but underestimates storm surge in regions where storm surges are dominantly induced by tropical cyclones and topographically complex areas, such as estuaries and semi-enclosed bays. As our global modeling capability and resolution improves, a later rerun of these analyses could improve understanding of future hazards. Future extensions of this work could consider the change in shoreline as sea level rises, particularly in closed embayments, and mitigation strategies based on changing the shoreline type.

Data Availability

The NTR coastal inundation layers, wave hazards and coastal flood hazard profiles for this region are available online for the public (Cook and Herdman, 2025).

Acknowledgements

We thank Kai Parker and Athina Lange our colleagues at U.S. Geological Survey who provided many helpful comments. We thank Leah Topping and Heather Moule for their efforts organizing the geographical figures. Any use of trade, firm, or product names is for descriptive purposes only and does not imply endorsement by the U.S. Government.

Tables

Table 1: Water Level Station List

	Station ID	Station Name	Lat	Lon	Record Length (years)	Last Date of Record	95% Threshold* (m)	Events per year above threshold	Historical AEP *(m)			
Source									0.99	0.1	0.04	0.01
NOAA	8518750	The Battery, NY	40.70	-74.02	97	31-Dec-2024	0.326	10.9	1.00	1.55	1.78	2.17
NOAA	8516945	Kings Point, NY	40.81	-73.77	26	31-Dec-2024	0.308	11.7	1.32	2.04	2.38	2.98
NOAA	8510560	Montauk, NY	41.05	-71.96	72	30-Nov-2024	0.269	11.2	0.826	1.26	1.43	1.71
NOAA	8516990	Willets Point, NY	40.79	-73.78	66	14-Nov-2000	0.369	11.1	1.22	2.04	2.41	2.99
NOAA	8465705	New Haven, CT	41.28	-72.91	25	30-Nov-2004	0.272	11.7	1.09	1.70	2.00	2.51
NOAA	8461490	New London, CT	41.372	-72.10	83	30-Nov-2024	0.272	11.3	0.855	1.30	1.49	1.78
NOAA	8467150	Bridgeport, CT	41.17	-73.18	54	30-Nov-2024	0.289	11.6	1.13	1.77	2.05	2.54
NOAA	8514560	Port Jefferson, NY	40.95	-73.08	33	01-Oct-1992	0.323	10.9	1.05	1.63	1.86	2.20
USGS	01194750	CONNECTICUT RIVER AT ESSEX, CT	41.35	-72.38	13	27-Dec-2022	0.359	8.02	0.888	1.51	1.82	2.36
USGS	01194796	CONNECTICUT RIVER AT OLD LYME, CT	41.31	-72.35	17	17-Jun-2024	0.305	10.2	0.863	1.53	1.87	2.51
USGS	01302250	EAST CREEK AT SANDS POINT NY	40.87	-73.71	15	02-Jul-2024	0.265	11.1	0.935	1.70	2.11	2.85
USGS	01311145	EAST ROCKAWAY INLET AT ATLANTIC BEACH NY	40.59	-73.74	14	13-Dec-2021	0.313	10.3	0.855	1.44	1.73	2.24
USGS	01302845	FROST CREEK AT SHEEP LN BRIDGE AT LATTINGTOWN NY	40.91	-73.59	14	26-Apr-2024	0.272	11.5	0.974	1.75	2.17	2.93
USGS	01309225	GREAT SOUTH BAY AT LINDENHURST NY	40.67	-73.36	13	07-Aug-2024	0.260	9.04	0.666	1.07	1.26	1.55
USGS	01311143	HOG ISLAND CHANNEL AT ISLAND PARK NY	40.61	-73.66	11	12-Jul-2023	0.357	9.25	0.984	1.55	1.79	2.17
USGS	01310521	HUDSON BAY AT FREEPORT NY	40.63	-73.58	14	10-Aug-2021	0.293	10.4	0.851	1.39	1.62	2.02
USGS	01311850	JAMAICA BAY AT INWOOD NY	40.62	-73.76	14	8-Jun-2022	0.309	10.8	0.963	1.61	1.93	2.46
USGS	01304200	ORIENT HARBOR AT ORIENT NY	41.1	-72.31	10	11-Jan-2024	0.286	10.9	0.937	1.63	1.95	2.51
USGS	01310740	REYNOLDS CHANNEL AT POINT LOOKOUT NY	40.59	-73.58	17	23-Sep-2024	0.301	10.2	0.86	1.36	1.56	1.90
USGS	01311875	ROCKAWAY INLET NEAR FLOYD BENNETT FIELD NY	40.57	-73.89	14	29-Dec-2023	0.315	10.5	0.924	1.59	1.93	2.52
USGS	01302600	WEST POND AT GLEN COVE NY	40.89	-73.64	11	30-Sep-2024	0.385	9.36	1.13	1.90	2.28	2.97

^{*}These starred columns report meters of NTR (non-tidal residual)

References

Almar, R., Ranasinghe, R., Bergsma, E. W. J., Diaz, H., Melet, A., Papa, F., et al. (2021). A global analysis of extreme coastal water levels with implications for potential coastal overtopping. *Nature Communications*, *12*(1), 3775. https://doi.org/10.1038/s41467-021-24008-9

- Barnard, P. L., Van Ormondt, M., Erikson, L. H., Eshleman, J., Hapke, C., Ruggiero, P., et al. (2014).

 Development of the Coastal Storm Modeling System (CoSMoS) for predicting the impact of storms on high-energy, active-margin coasts. *Natural Hazards*, *74*(2), 1095–1125.

 https://doi.org/10.1007/s11069-014-1236-y
- Blue Marble Geographics. (2024, February 14). Global Mapper Pro (Version 25.1.0(64-bit)). Hallowell,

 Maine: Blue Marble Geographics. Retrieved from https://www.bluemarblegeo.com/
- Chen, C., Huang, H., Beardsley, R. C., Liu, H., Xu, Q., & Cowles, G. (2007). A finite volume numerical approach for coastal ocean circulation studies: Comparisons with finite difference models.

 Journal of Geophysical Research: Oceans, 112(C3), 2006JC003485.

 https://doi.org/10.1029/2006JC003485
- Cialone, M.A., Massey, T.C., Anderson, M.E., Grzegorzewski, A.S., Jensen, R.E., Cialone, A., et al. (2015).

 North Atlantic Coast Comprehensive Study (NACCS) coastal storm model simulations: Waves and water levels (No. ERDC/CHL TR-15-14). U.S. Army Engineer Research and Development Center, Coastal and Hydraulics Laboratory. Retrieved from https://usace.contentdm.oclc.org/digital/collection/p266001coll1/id/3681/
- Codiga, D. L. (2011). Unified tidal analysis and prediction using the UTide Matlab functions. Graduate School of Oceanography, University of Rhode Island.

 https://doi.org/10.13140/RG.2.1.3761.2008
- Coles, S. (2001). Multivariate Extremes. In S. Coles, *An Introduction to Statistical Modeling of Extreme Values* (pp. 142–168). London: Springer London. https://doi.org/10.1007/978-1-4471-3675-0_8
- Cook, S.E. and Herdman, L.M., 2025, Geospatial dataset of coastal-inundation maps for Long Island and Long Island Sound (CT/NY): U.S. Geological Survey data release, https://doi.org/10.5066/P94P4WXX.

- Crawford, A. D., McCrystall, M. R., Lukovich, J. V., & Stroeve, J. C. (2023). The Response of Extratropical Cyclone Propagation in the Northern Hemisphere to Global Warming. *Journal of Climate*, *36*(20), 7123–7142. https://doi.org/10.1175/JCLI-D-23-0082.1
- Danielson, J. J., Poppenga, S. K., Brock, J. C., Evans, G. A., Tyler, D. J., Gesch, D. B., et al. (2016).

 Topobathymetric Elevation Model Development using a New Methodology: Coastal National Elevation Database. *Journal of Coastal Research*, 76, 75–89. https://doi.org/10.2112/SI76-008
- Davison, A. C., & Smith, R. L. (1990). Models for Exceedances Over High Thresholds. *Journal of the Royal Statistical Society Series B: Statistical Methodology*, *52*(3), 393–425. https://doi.org/10.1111/j.2517-6161.1990.tb01796.x
- EC-Earth Consortium (EC-Earth). (2018). EC-Earth-Consortium EC-Earth3P-HR model output prepared for CMIP6 HighResMIP (Version 20241021) [Application/x-netcdf]. Earth System Grid Federation. https://doi.org/10.22033/ESGF/CMIP6.2323
- England, J. F. Jr., Cohn, T. A., Faber, B. A., Stedinger, J. R., Thomas Jr., W. O., Veilleux, A. G., et al. (2018). *Guidelines for determining flood flow frequency Bulletin 17C* (Report No. 4-B5, Version 1.1:

 May 31, 2019) (p. 168). Reston, VA. https://doi.org/10.3133/tm4B5
- Esri. (2024). ArcGIS Pro: Esri Software release (Version 3.3.0).
- Eurotop II. (2018). Manual on wave overtopping of sea defences and related structures. An overtopping manual largely based on European research, but for worldwide application (Manual No. Second Edition 2018). Retrieved from www.overtopping-manual.com
- FEMA. (2013, July 8). National Flood Hazard Layer (NFHL).
- Frederikse, T., Landerer, F., Caron, L., Adhikari, S., Parkes, D., Humphrey, V. W., et al. (2020). The causes of sea-level rise since 1900. *Nature*, *584*(7821), 393–397. https://doi.org/10.1038/s41586-020-2591-3

- Haarsma, R. J., Roberts, M. J., Vidale, P. L., Senior, C. A., Bellucci, A., Bao, Q., et al. (2016). High

 Resolution Model Intercomparison Project (HighResMIP v1.0) for CMIP6. *Geoscientific Model*Development, 9(11), 4185–4208. https://doi.org/10.5194/gmd-9-4185-2016
- Hu, L., Nikolopoulos, E. I., Marra, F., & Anagnostou, E. N. (2020). Sensitivity of flood frequency analysis to data record, statistical model, and parameter estimation methods: An evaluation over the contiguous United States. *Journal of Flood Risk Management*, *13*(1), e12580. https://doi.org/10.1111/jfr3.12580
- Ilia, A., Cifuentes-Lorenzen, A., McCardell, G., & O'Donnell, J. (2023). Wind Wave Growth and Dissipation in a Narrow, Fetch-Limited Estuary: Long Island Sound. *Journal of Marine Science and Engineering*, 11(8), 1579. https://doi.org/10.3390/jmse11081579
- Liu, C., Jia, Y., Onat, Y., Cifuentes-Lorenzen, A., Ilia, A., McCardell, G., et al. (2020). Estimating the Annual Exceedance Probability of Water Levels and Wave Heights from High Resolution Coupled Wave-Circulation Models in Long Island Sound. *Journal of Marine Science and Engineering*, 8(7), 475. https://doi.org/10.3390/jmse8070475
- Mazas, F., & Hamm, L. (2011). A multi-distribution approach to POT methods for determining extreme wave heights. *Coastal Engineering*, *58*(5), 385–394. https://doi.org/10.1016/j.coastaleng.2010.12.003
- Mikolajewicz, U., Santer, B. D., & Maier-Reimer, E. (1990). Ocean response to greenhouse warming.

 Nature, 345(6276), 589–593. https://doi.org/10.1038/345589a0
- Muis, S, Irazoqui Apecechea, M., Antolínez, J. A. A., Verlaan, M., Yan, K., & Dullaart, J. (2022a). Global sea level change indicators from 1950 to 2050 derived from reanalysis and high resolution CMIP6 climate projections [Data set]. Copernicus Climate Change Service (C3S) Climate Data Store (CDS). https://doi.org/10.24381/cds.6edf04e0

- Muis, S., Irazoqui Apecechea, M., Antolínez, J. A. A., Verlaan, M., Yan, K., & Dullaart, J. (2022b). Global sea level change time series from 1950 to 2050 derived from reanalysis and high resolution CMIP6 climate projections [Data set]. Copernicus Climate Change Service (C3S) Climate Data Store (CDS). https://doi.org/doi.org/10.24381/cds.a6d42d60
- Muis, Sanne, Apecechea, M. I., Dullaart, J., De Lima Rego, J., Madsen, K. S., Su, J., et al. (2020). A High-Resolution Global Dataset of Extreme Sea Levels, Tides, and Storm Surges, Including Future

 Projections. *Frontiers in Marine Science*, 7, 263. https://doi.org/10.3389/fmars.2020.00263
- Nadal-Caraballo, N. C., Melby, J. A., & Gonzalez, V. M. (2016). Statistical Analysis of Historical Extreme

 Water Levels for the U.S. North Atlantic Coast Using Monte Carlo Life-Cycle Simulation. *Journal of Coastal Research*, 32(1), 35–45. https://doi.org/10.2112/JCOASTRES-D-15-00031.1
- National Geodetic Survey (NGS). (2023). NOAA Continually Updated Shoreline Product (CUSP), [Data set]. https://shoreline.noaa.gov/data/datasheets/cusp.html. Retrieved from https://shoreline.noaa.gov/data/datasheets/cusp.html
- Nederhoff, K., Saleh, R., Tehranirad, B., Herdman, L., Erikson, L., Barnard, P. L., & Van Der Wegen, M. (2021). Drivers of extreme water levels in a large, urban, high-energy coastal estuary A case study of the San Francisco Bay. *Coastal Engineering*, *170*, 103984. https://doi.org/10.1016/j.coastaleng.2021.103984
- Nederhoff, K., Leijnse, T. W. B., Parker, K., Thomas, J., O'Neill, A., Van Ormondt, M., et al. (2024).
 Tropical or extratropical cyclones: what drives the compound flood hazard, impact, and risk for the United States Southeast Atlantic coast? *Natural Hazards*, 120(9), 8779–8825.
 https://doi.org/10.1007/s11069-024-06552-x

NOAA (National Oceanic and Atmospheric Administration), 2025, *Tides & Currents*. Accessed [March 11,2025]. https://tidesandcurrents.noaa.gov/

- O'Neill, B. C., Tebaldi, C., van Vuuren, D. P., Eyring, V., Friedlingstein, P., Hurtt, G., et al. (2016). The Scenario Model Intercomparison Project (ScenarioMIP) for CMIP6. *Geoscientific Model Development*, *9*(9), 3461–3482. https://doi.org/10.5194/gmd-9-3461-2016
- Owen, M. W. (1980). *Design of seawalls allowing for wave overtopping* (No. Report EX 924). HR Wallingford.
- Pedregosa, F., Varoquaux, G., Gramfort, A., Michel, V., Thirion, B., Grisel, O., ... & Duchesnay, É. (2011).

 Scikit-learn: Machine learning in Python. *Journal of Machine Learning Research*, 12, 2825–2830.
- Pickands, J., III. (1975). Statistical Inference Using Extreme Order Statistics. *The Annals of Statistics*, *3*(1). https://doi.org/10.1214/aos/1176343003
- Pugh, D. T. (1987). *Tides, surges and mean sea-level*. Chichester New York Brisbane [etc.]: J. Wiley and sons.
- Roberts, M. (2017a). MOHC HadGEM3-GC31-HM model output prepared for CMIP6 HighResMIP (2017b)

 (Version 20230220) [Application/x-netcdf]. Earth System Grid Federation.

 https://doi.org/10.22033/ESGF/CMIP6.446
- Roberts, M. (2017b). MOHC HadGEM3-GC31-MM model output prepared for CMIP6 HighResMIP (2017a) (Version 20230720) [Application/x-netcdf]. Earth System Grid Federation. https://doi.org/10.22033/ESGF/CMIP6.1902
- Roberts, M. J., Camp, J., Seddon, J., Vidale, P. L., Hodges, K., Vannière, B., et al. (2020). Projected Future

 Changes in Tropical Cyclones Using the CMIP6 HighResMIP Multimodel Ensemble. *Geophysical Research Letters*, 47(14), e2020GL088662. https://doi.org/10.1029/2020GL088662
- Scoccimarro, E., Bellucci, A., & Peano, D. (2017). CMCC CMCC-CM2-VHR4 model output prepared for CMIP6 HighResMIP (Version 20220628) [Application/x-netcdf]. Earth System Grid Federation. https://doi.org/10.22033/ESGF/CMIP6.1367

- Stockdon, H. F., Holman, R. A., Howd, P. A., & Sallenger, A. H. (2006). Empirical parameterization of setup, swash, and runup. *Coastal Engineering*, *53*(7), 573–588.

 https://doi.org/10.1016/j.coastaleng.2005.12.005
- Sweet, W., Hamlington, B., Kopp, R. E., Weaver, C., Barnard, P. L., Bekaert, D., et al. (2022). *Global and regional sea level rise scenarios for the United States* (Report). Retrieved from https://pubs.usgs.gov/publication/70229139
- U.S. Army Corps of Engineers. (1995). *Design of Coastal Revetments, Seawalls, and Bulkheads*. (No. EM 1110-2-1614).
- U.S. Geological Survey, 2025, *USGS Water Data for the Nation: National Water Information System database*. https://doi.org/10.5066/F7P55KJN (accessed March 11,2025)
- Vecchi, G. A., Landsea, C., Zhang, W., Villarini, G., & Knutson, T. (2021). Changes in Atlantic major hurricane frequency since the late-19th century. *Nature Communications*, *12*(1), 4054. https://doi.org/10.1038/s41467-021-24268-5
- Vitousek, S., Barnard, P. L., & Limber, P. (2017a). Can beaches survive climate change? *Journal of Geophysical Research: Earth Surface*, 122(4), 1060–1067.

 https://doi.org/10.1002/2017JF004308
- Vitousek, S., Barnard, P. L., Fletcher, C. H., Frazer, N., Erikson, L., & Storlazzi, C. D. (2017b). Doubling of coastal flooding frequency within decades due to sea-level rise. *Scientific Reports*, 7(1), 1399. https://doi.org/10.1038/s41598-017-01362-7
- Warner, J. C. (2022). Collection of COAWST model forecast for the US East Coast and Gulf of Mexico [Data set]. U.S. Geological Survey. https://doi.org/10.5066/P903KPBJ

- Warner, J. C., Armstrong, B., He, R., & Zambon, J. B. (2010). Development of a Coupled Ocean–
 Atmosphere–Wave–Sediment Transport (COAWST) Modeling System. *Ocean Modelling*, *35*(3), 230–244. https://doi.org/10.1016/j.ocemod.2010.07.010
- Zhang, C., & Li, C. (2019). Effects of hurricane forward speed and approach angle on storm surges: an idealized numerical experiment. *Acta Oceanologica Sinica*, *38*(7), 48–56. https://doi.org/10.1007/s13131-018-1081-z
- Zhao, M., Golaz, J. -C., Held, I. M., Guo, H., Balaji, V., Benson, R., et al. (2018). The GFDL Global

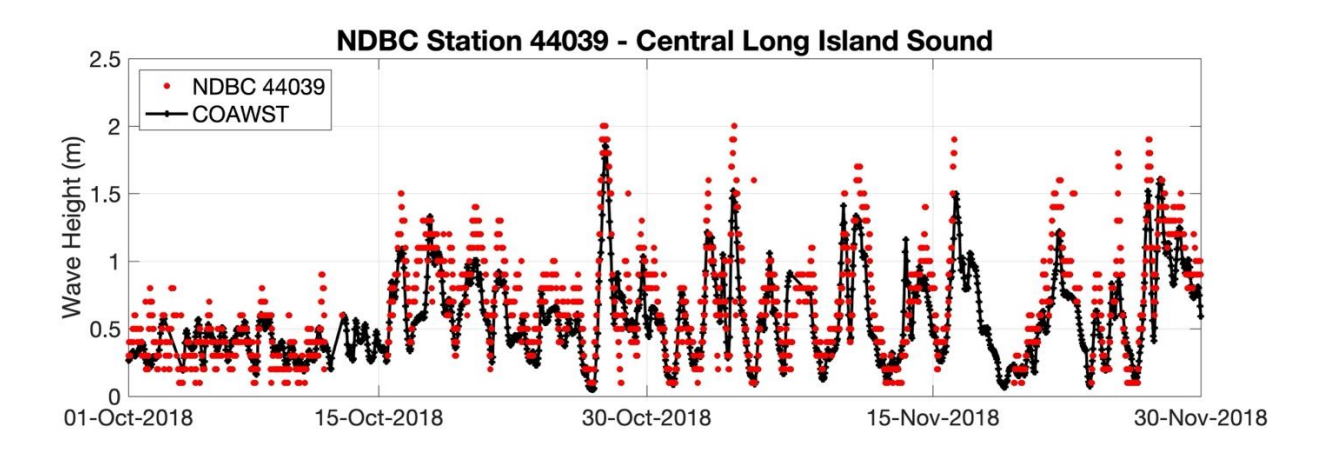
 Atmosphere and Land Model AM4.0/LM4.0: 2. Model Description, Sensitivity Studies, and

 Tuning Strategies. *Journal of Advances in Modeling Earth Systems*, 10(3), 735–769.

 https://doi.org/10.1002/2017MS001209

APPENDICES

Appendix 1: COAWST validation for waves



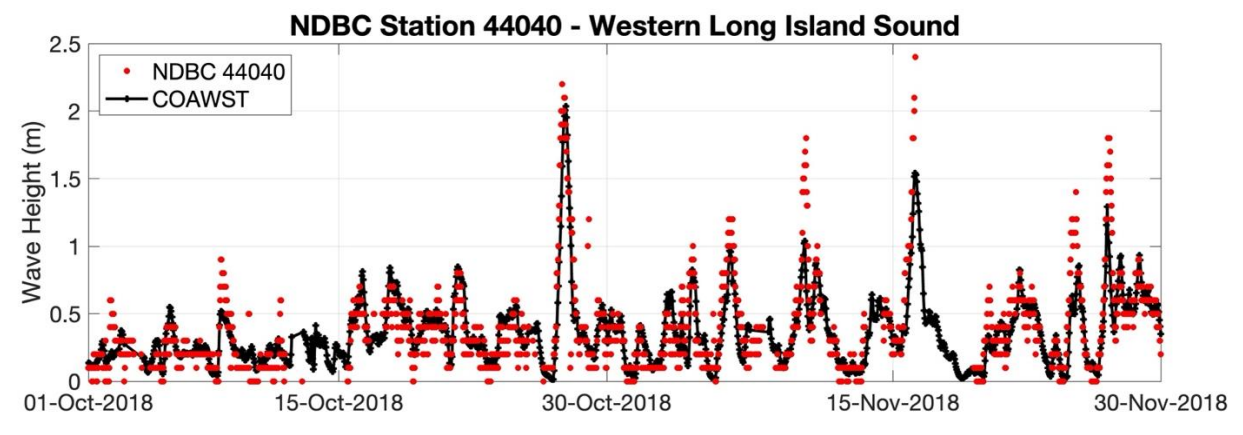


Figure A1: Times series comparing wave height (m) between COAWST model output and observations for central Long Island Sound (NDBC Buoy 44039; top panel) and western Long Island Sound (NDBC Buoy 44040; bottom panel). Buoy locations shown with yellow stars on Figure 1.

Appendix 2: GPD Fit to all stations in Table 1

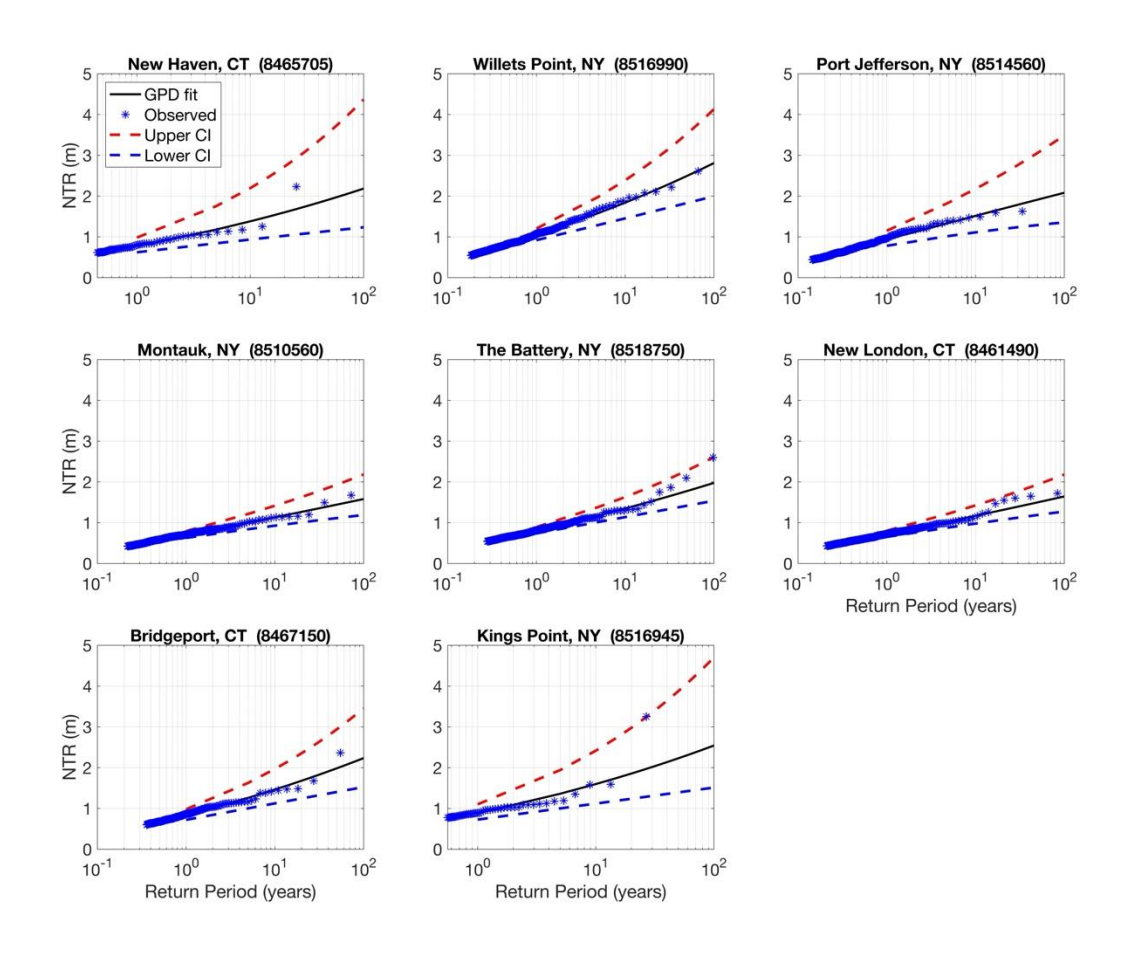


Figure A2a: GPD fits for NOAA stations listed in Table 1

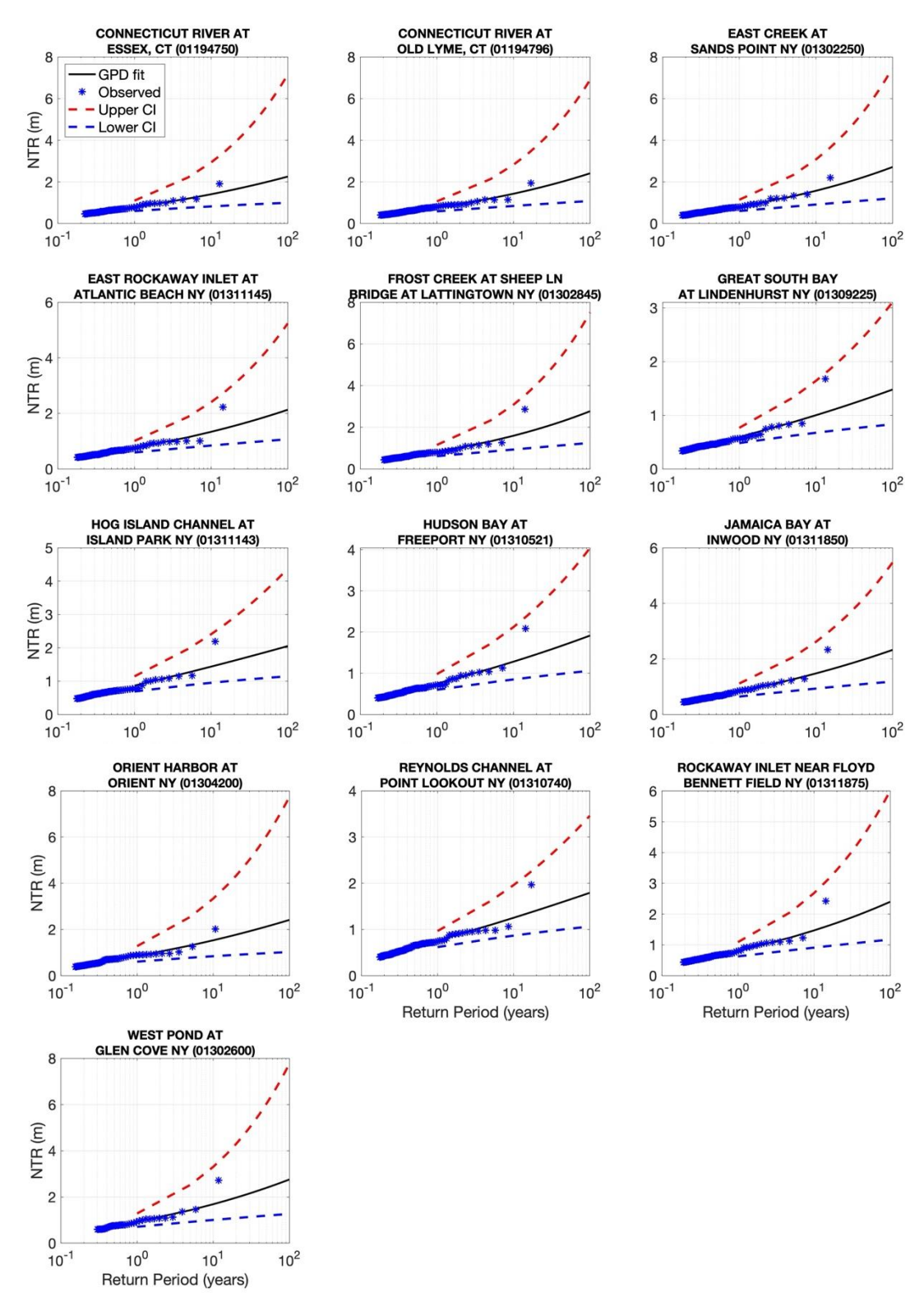


Figure A2b: GPD fits for USGS stations listed in Table 1.

Appendix 3: FEMA Validation Plot

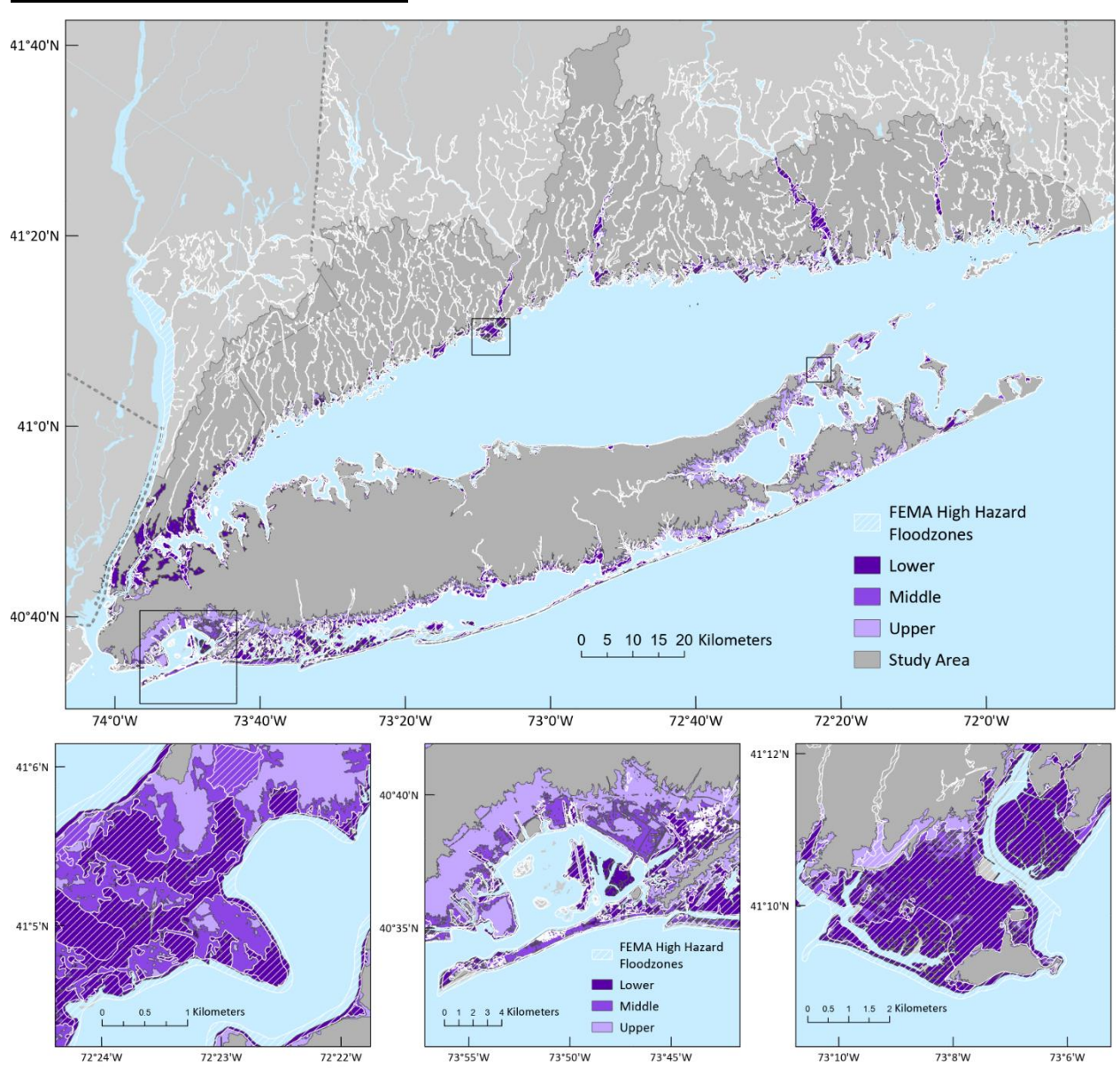


Figure A3: AEP 0.01 compared with the FEMA flood layer (FEMA, 2013).

Appendix 4: Hazard Ranking Methodology

To create a coastal hazard ranking for each cell of the 900 square meter grid, the percent of each grid cell inundated under each AEP scenario was computed. If the cell did not flood, even under the upper confidence limit of the 100 year flood, it was not ranked for having a coastal flood hazard. The cells that remained were grouped by percent inundated under the different inundation scenarios to find the natural breaks in the distribution. The average percent inundated for the expected 100-year return period is provided in parentheses for each given hazard level: 1 (3%), 2 (10%), 3 (52%), 4 (76%) and 5 (96%). Refer to the final coastal inundation ranking in panel a of Figure A3.

The wave ranking is based upon the discharge thresholds identified in Eurotop II (2018). The median value of the discharges in each grid cell from the different scenarios considered was used to assign the wave ranking. The following ranges of discharge correspond to sequentially increasing rankings (1-5); less than 0.1 L/s, 0.1 to 1 L/s, 1 to 10 L/s, 10 to 100 L/s, greater than 100 L/s.

The coastal ranking was assigned based on combining the two scores. If the grid cell only received one ranking (either wave or inundation) its final ranking was set to that ranking. If a grid cell had both coastal and wave rankings, the final ranking was the average of the two rankings, rounding up to the nearest integer.

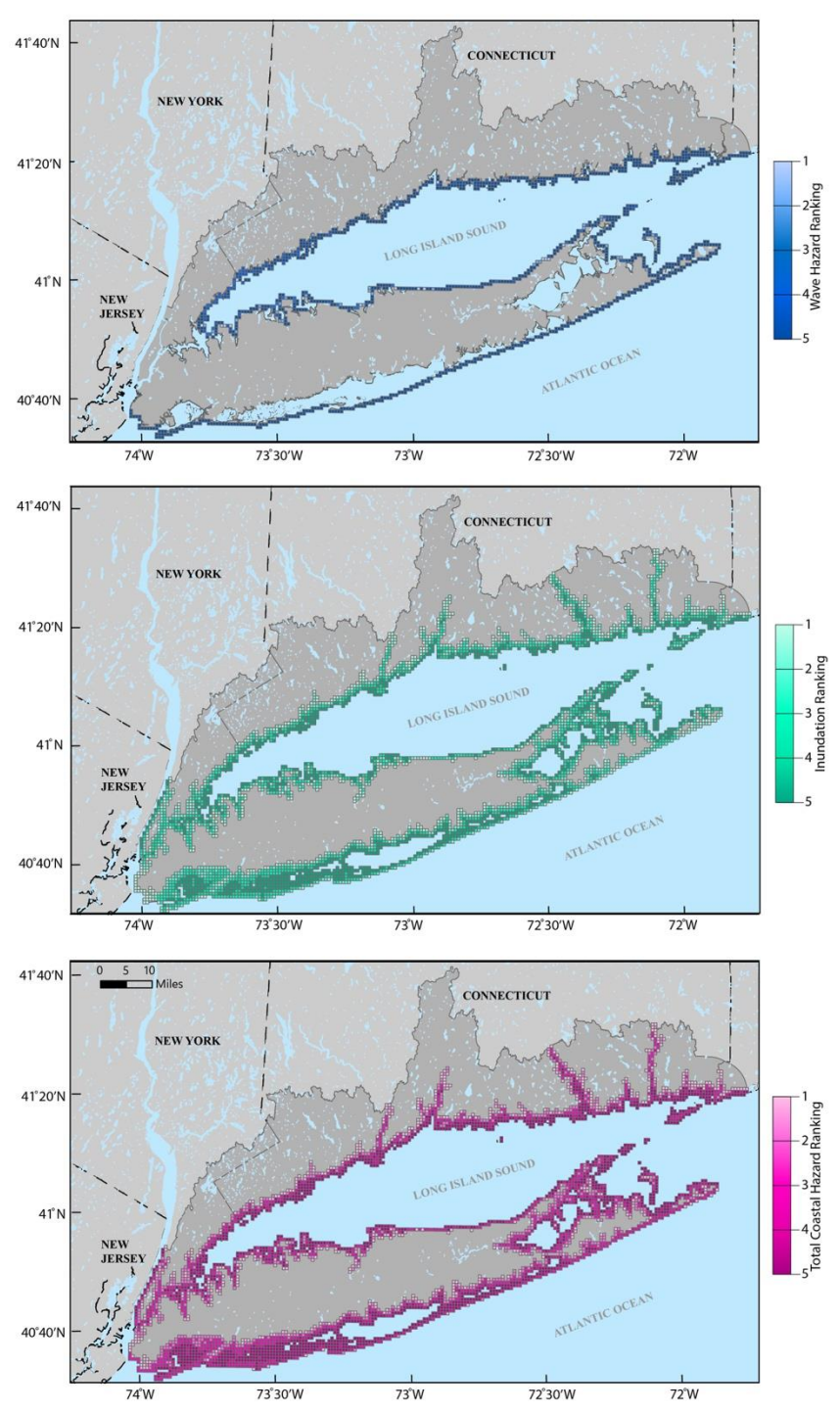


Figure A4: a) Inundation Ranking b) Wave Hazard Ranking c) Total Coastal Hazard ranking. Base map from U.S. Geological Survey National Atlas digital data, 1:1,000,000 scale